FOUNDATION FOR RESEARCH AND TECHNOLOGY - HELLAS

MASTER THESIS

- Skyrmionic Textures and Applications

Michael Lianeris

University of Crete , UOC

Deparment of Applied Mathematics

Academic Year 2021 - 2022

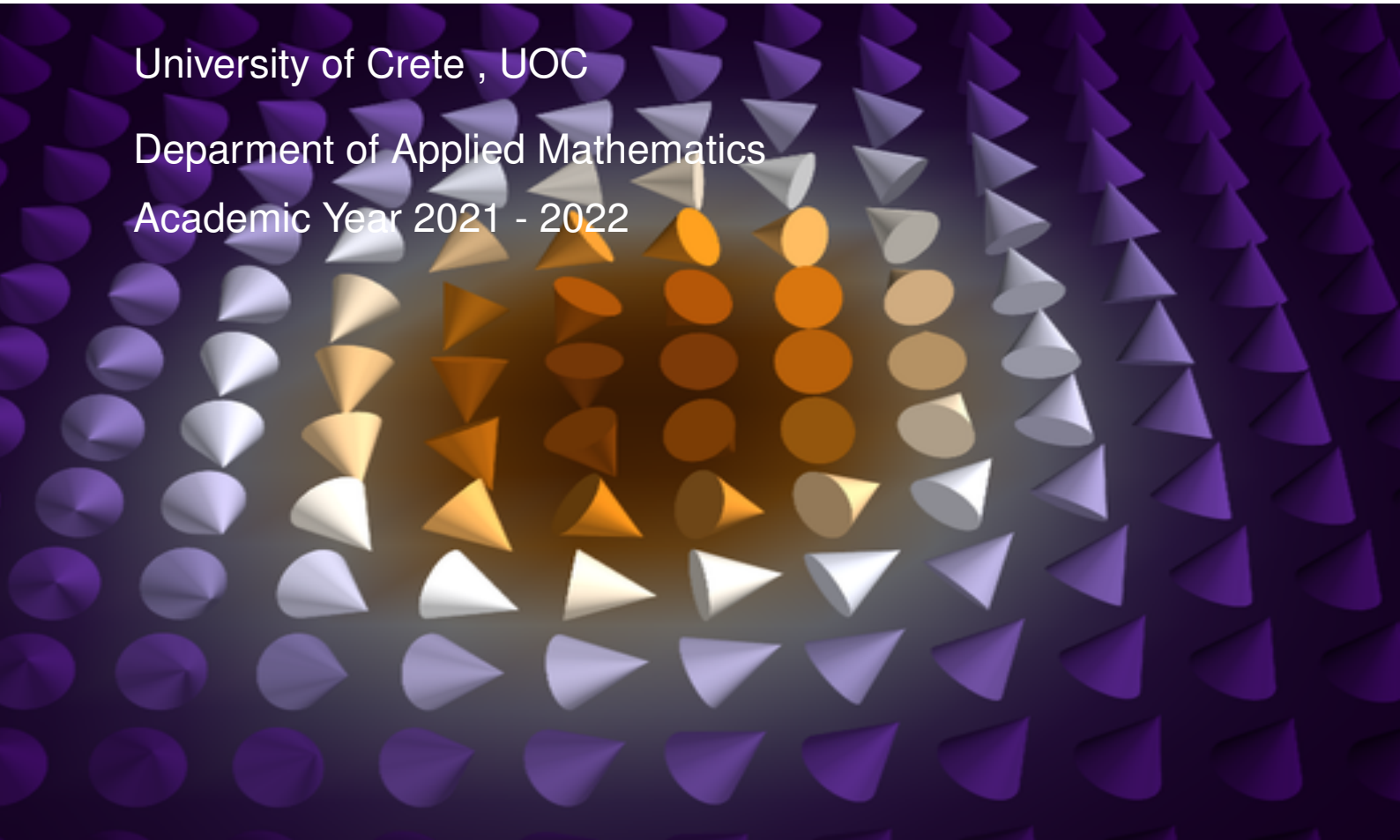

Contents

Chapter 1

Introduction

1.1 History of Skyrmions

Skyrmions are named after the British nuclear physicist Tony Skyrme who first proposed their existence in 1961 [1]. His idea was to model subatomic entities like protons and neutrons using convoluted twists in the quantum field that describe the particles. While the concept was useful in many ways, such as accurately predicting some of the properties of fundamental particles like quarks and gluons, it struggled with other aspects of nuclear behavior.

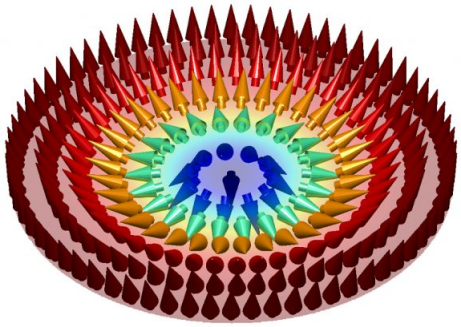

Figure 1.1: Graphic representation of a skyrmion.

The Skyrme model is a non-linear field theory for pions in 3+1 dimensions with soliton solutions called Skyrmions . Suitably quantised Skyrmions are models for physical baryons. Skyrme's theory is non-integrable and therefore progress in understanding Skyrmion dynamics has depended on numerical simulations, approximation schemes or a combination of both. This approach has been quite successful in the study of static soliton solutions in Skyrme's theory .

1.2 Magnetic Skyrmions

Chiral magnetic skyrmions are topological magnetic configurations that are stabilised in materials with the Dzyaloshinskii-Moriya interaction. They have been observed in a number of experiments and the detailed features of individual skyrmions have been resolved experimentally to an impressive degree for isolated skyrmions and in a skyrmion lattice . The experimental works have mapped the profile of the skyrmion, i.e., the magnetization as a function of the distance from its center. The skyrmion profile is the foundation for the study of the statics and of dynamical behaviors of skyrmions and the subsequent derivation of quantitative results.

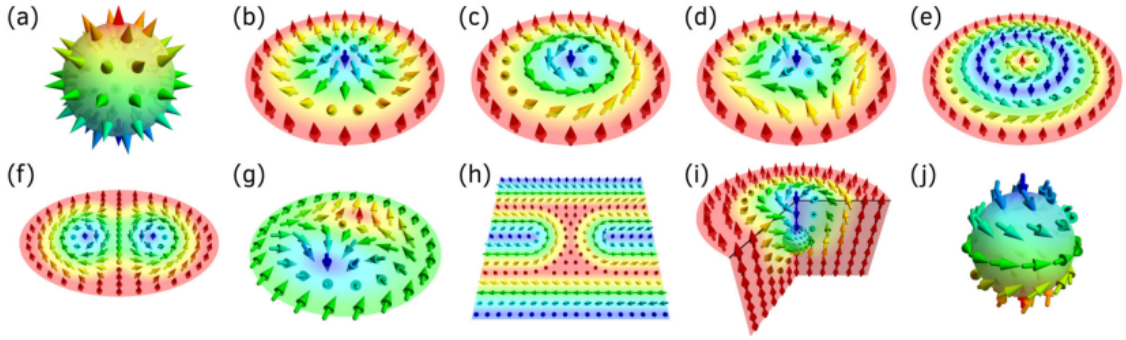

Figure 1.2: Zoo of (topological) spin textures with different winding numbers. (a) Hedgehog, (b) Néel-type skyrmion, (c) Bloch-type skyrmion, (d) antiskyrmion, (e) skyrmionium, (f) biskyrmion, (g) example of an in-plane skyrmion, (h) skyrmion in helical background, (i) chiral bobber, (j) combed anti-hedgehog formed around the Bloch point in pane. [Source [2].]

Although skyrmions were predicted a long time ago,experimentally these chiral spin-structures have been only observed less than ten years ago in bulk, thin films,and monolayers.Since then, a variety of novel (topological) magnetic textures have been observed, see Fig. 1.2 shows a couple of examples. Some of these will be discussed in detail later in this Thesis.

Concerning what constitutes a skyrmion, in the community, there are different definitions used. The term itself was introduced in relation to Skyrme's original work in nuclear physics where he investigated topologically non-trivial localized field solutions of a non-linear sigma model to describe elementary particles. Since there is no obvious distinction for what should be called a skyrmion in condensed matter physics, within this article, we define a skyrmion as being any spin structure in which the center magnetization is in the opposite direction to its boundary and which can be mapped once to the sphere Fig. 1.3.

A classification of spin structures can be based on their topology, which often has direct consequences for the physical properties of magnetic textures and measurable quantities like Hall resistances. Effective two dimensional textures described by a local magnetization direction $\mathbf{m}$ can be classified by the skyrmion number [Appendix B]

$$Q = \frac{1}{4\pi} \int \mathbf{m} \cdot (\partial_x \mathbf{m} \times \partial_y \mathbf{m}) \quad dxdy \tag{1.2.1}$$

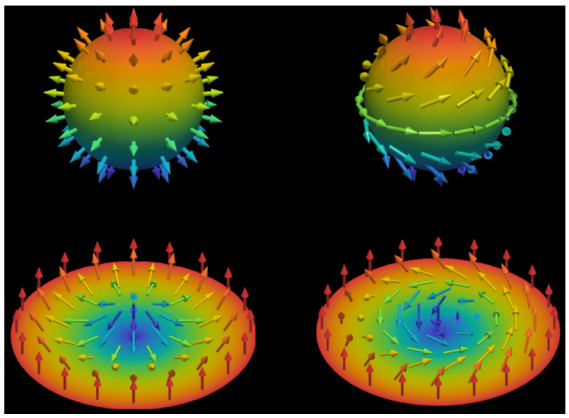

Figure 1.3: The stereographic projection , where it becomes a skyrmion. The left-hand version is a Néel skyrmion , the right-hand version, where the spins have been combed over, is a Bloch skyrmion.[Source [3].]

We note that topology is a mathematical concept for continuous systems that defines two structures to be equivalent if a continuous mapping from one to the other exists. In contrast, real physical systems are usually discrete, for example, due to the underlying atomic lattice. Naturally, this implies that topologically non-conserving transformations are allowed but have a finite, non-zero energy penalty that must be overcome. In general, the understanding of convoluted spin textures is based on the idea of the interplay of different interactions and their relative strengths.

1.3 Applications

1.3.1 Skyrmionic logic devices

The fact that a skyrmion can be regarded as an independent 'particle' has also given rise to the proposal of several conceptual devices of skyrmion-based spin logic devices. Most of them rely on the results demonstrated through micromagnetic simulations performed in nanoscale wires having different widths, that a single skyrmion can be transformed into a domain-wall pair and vice versa. This conversion mechanism allows in principle to duplicate or to merge skyrmions at will through the design of specific nanostructures and thus to perform basic logic operations. Based on these additional functionalities have recently conceptualized skyrmion logic gates AND and OR, and thus realized the first step toward a complete logical architecture with the objectives to overtake the existing spin logic devices, particularly in their level of integration.

1.3.2 Skyrmion magnonic crystal

The ability to control spatially the nucleation of skyrmions, for example through either a local application of a magnetic or electric field or the injection of spin polarized current give also the opportunity to prepare an artificial periodic arrangement of skyrmions in a 1D or 2D nanostructure.

Such skyrmion lattices can then be used as periodic modulation of the magnetization to tailor the propagation of spin waves inside this novel type of "metamaterial". Indeed has recently shown through numerical simulations that a strong advantage of such skyrmion-based magnonic crystal compared to more standard ones (based on periodic modulation of the magnetic properties induced usually by lithography process) is that it can be dynamically reconfigured simply by changing the diameter of the skyrmions (by applying a magnetic field) or by changing the periodicity of the lattice or even erase it (Fig. 1.4).

Note also that skyrmion crystals at the scale of the nanometer can be envisaged, what is unreachable for conventional magnonic crystal fabricated with the existing lithography techniques. Leveraging of such functionality should thus allow a dynamical switching between full rejection and full transmission of spin waves in a waveguide. Besides the benefit for magnonic devices, it has been recently shown that the spin waves themselves might be in a topological phase when propagating in a 2D atomic scale skyrmion lattice which should allow the realization of the spin-wave analogue of the anomalous quantum Hall effect for electrons.

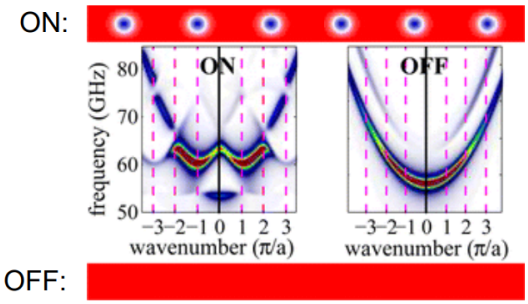

Figure 1.4: A skyrmion lattice could form an ideal magnonic crystal with extremely small dimensions, unreachable with conventional lithography.[Source [4].]

1.3.3 Skyrmion-based rf devices

A class of components for which the topological nature of skyrmions could have practical applications is in nanoscale radio frequency devices.. For example, a dynamical mode of a single skyrmion in a dot that is typical of its topological nature is the low frequency. It has been proposed that the skyrmion breathing mode induced by spin torques can be used to generate a rf signal if the dot with a skyrmion is part of a magnetoresistive device such as a spin valve or a magnetic tunnel junction (see Fig. 1.5) . One of the advantages of the resulting skyrmion-based spin torque oscillator, compared for example to a vortex based spin torque oscillator, can be that the skyrmion, being a localized soliton, will be less sensitive to external perturbation and thus display a more coherent dynamic.

Another function numerically investigated is the concept of skyrmion-based microwave detector, which relies on the resonant excitation of the breathing mode when the frequency of the external rf signal equals the frequency of the breathing mode (that can be largely changed by the application of an external perpendicular field for example) and the conversion of this resonant dynamics into a dc mixed voltage.

Finally, a novel type of skyrmion-based spin torque oscillator is based on the self-sustained gyration arising from the competition between the confinement from the boundary edges and the spin forces due to an inhomogeneous spin polarizer. The associated gyrotropic frequency is lower by about one order of magnitude compared to conventional vortex based spin torque oscillators but their main advantage is that there is no threshold current for the onset of the skyrmion dynamics.

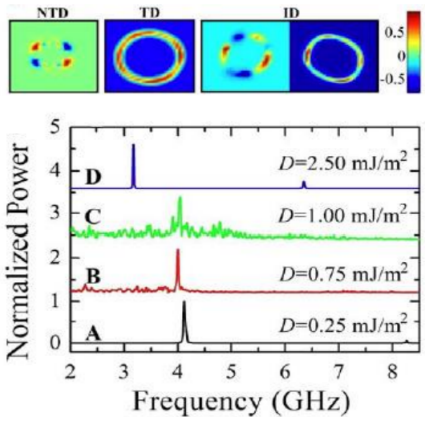

Figure 1.5: Different excitation modes of the skyrmions could be used to fabricate radiofrequency filters.[Source [4].]

Chapter 2

Exchange interaction

2.1 Magnetic Moments of Atoms

In classical electromagnetism we may consider a current in a closed loop . The magnetic moment is defined as an integral over the loop

$$\mu = \oint_C \mathbf{r} \times d\mathbf{s}, \tag{2.1.1}$$

where I is the current units $(\mathrm{A/m^2})$. A useful form of the magnetic moment in Eq. (2.1.1) is

$$\mu = I \int_A d\alpha = IA\hat{n}. \tag{2.1.2}$$

where A denotes both the surface enclosed by the loop C and the area of this domain, and $\hat{n}$ is the directed normal to the surface A. Eq. (2.1.1) shows that the magnetic moment μ associated with an orbiting electron is proportional to the angular momentum $\mathbf{L}$ of the electron motion. Thus we write

$$\mu = \gamma \mathbf{L}, \tag{2.1.3}$$

where $\gamma = g_e|e|/2m_e$ is the gyromagnetic ratio. The charge and mass of the electron are e, m_e , while g_e is the Landé factor which may take values different than unity depending on whether the magnetic moment is due to pure orbital motion or to the electron spin angular momentum.The energy $\mathbf{E}$ of a magnetic moment in a magnetic field $\mathbf{B}$ is

$$\mathbf{E} = -\mu \mathbf{B}. \tag{2.1.4}$$

This shows that the energy is minimized when the magnetic moment is aligned with the magnetic field. As the magnitude of the magnetic moment is constant (and we assume a constant in time magnetic field), we may write $\mathbf{E} = -\mu \mathbf{B} \cos\psi$, where ψ is the angle between μ and $\mathbf{B}$. We define a torque with magnitude

$$\tau = -\frac{\partial \mathbf{E}}{\partial \psi} = -\mu \mathbf{B} \sin\psi, \tag{2.1.5}$$

and note that this is equal to $-|\mu \times \mathbf{B}|$. The direction of the torque should be perpendicular to both μ (as it's magnitude should remain constant) and to $\mathbf{B}$ as the energy, and thus the angle ψ , should be conserved. We can finally write

$$\tau = \mu \times \mathbf{B}. \tag{2.1.6}$$

(The sign of the above relation is chosen so that the force derived from the energy be $\mathbf{F} = -\nabla \mathbf{E}$.) We can now write an equation for the time derivative of the angular momentum or, more conveniently, of the magnetic moment

$$\frac{d\mu}{dt} = \gamma \mu \times \mathbf{B}. \tag{2.1.7}$$

Let us now assume a constant magnetic field $\mathbf{B}$,and let us suppose a coordinate system where we set the axis z in the direction of the field $\mathbf{B} = \mathbf{B}\hat{z}$. We write $\mu = (\mu_x, \mu_y, \mu_z)$ and then (2.1.7) reads

$$\begin{cases} \dot{\mu}_x &= \gamma B \mu_y \\ \dot{\mu}_y &= -\gamma B \mu_x \\ \dot{\mu}_z &= 0 \end{cases} \tag{2.1.8}$$

The solution to the latter system of equations is

$$\begin{cases} \mu_x &= \sin\theta \cos(\omega_L t) \\ \mu_y &= \sin\theta \sin(\omega_L t) \\ \mu_z &= \mu \cos\theta \end{cases}$$

where θ is the angle between μ and $\mathbf{B}$, and $\omega_L = \mu \mathbf{B}$ is called the Larmor precession frequency. We thus see that μ_z remains constant while the component of the magnetic moment perpendicular to the external field is precessing around the vector $\mathbf{B}$.

2.2 A chain of spins

A ferromagnetic material is characterized by the property that neighbouring magnetic moments tend to be aligned with each other. The magnetic moments are primarily due to the spin of electrons. For a chain of magnetic spins (moments) $\mathbf{S}_i$ an interaction which favours alignment of spins is typically expressed by the exchange interaction of the form [5]

$$E_{ex} = -J \sum \mathbf{S}_i \cdot \mathbf{S}_{i+1} = -\frac{J}{2} \sum \mathbf{S}_i \cdot (\mathbf{S}_{i+1} + \mathbf{S}_{i-1}), \tag{2.2.1}$$

where J is the exchange constant. If the two electrons are on the same atom the exchange integral is usually positive. This stabilizes the triplet state, and ensures an antisymmetric spatial state which minimizes the Coulomb repulsion between the two electrons by keeping them apart. This is consistent with Hund's first rule. When the electrons are on neighbouring atoms, the situation is very different. Any joint state will be a combination of a state centred on one atom and a state centred on the other atom. It is worth remembering that the energy of a particle in a one dimensional box of length L is proportional to L^{-2}. This is a kinetic energy and hence demonstrates that there is a large kinetic energy associated with being squized into a small box. The electrons therefore can save kinetic energy by forming bonds because this allows them to wander around both atoms rather than just one. The correct states to consider now are not atomic orbitals but molecular orbitals. These can be bonding or spatially symmetric, or andibonding-spatially antisymmetric, with the andibonding orbitals more energetically costly. This is because the antibomding orbital has a greater curvature and hence a larger kinetic energy. This favours singlet (antisymmetric) states and the exchange integral, therefore, is expected to be negative .

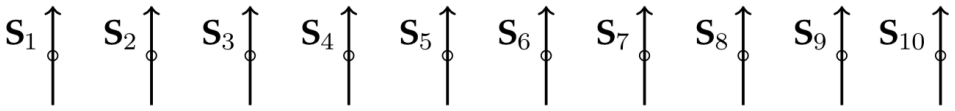

Figure 2.1: The figure represent an chain of fully aligned spins.

For the exchange energy, we obtain a minimum if all spins are aligned, $\mathbf{S}_i = \mathbf{S}_0$ where $\mathbf{S}_0 = \pm(0, 0, s)$ is a constant vector. Indeed,if we assume that $\mathbf{S}_i \,||\, \mathbf{S}_{i+1}$ then, from the definition of the dot product we get

$$\mathbf{S}_i \cdot \mathbf{S}_{i+1} = |\mathbf{S}_i| \cdot |\mathbf{S}_{i+1}| \cos\theta, \tag{2.2.2}$$

where θ is the angle between $\mathbf{S}_i$ and $\mathbf{S}_{i+1}$, and we have that $\theta = 0$. Therefore, we have that $\mathbf{S}_i \cdot \mathbf{S}_{i+1} = |\mathbf{S}_i| \cdot |\mathbf{S}_{i+1}|$ also assume that the length of the spins is constant, $|\mathbf{S}_1| = \cdots = |\mathbf{S}_n| = s$. and if we take the sum, for all i, we have the total energy has a minimum

$$E_{\text{ex}} = -J(N-1)s^2 \approx -JNs^2 \quad \text{for} \quad N \gg 1 \tag{2.2.3}$$

The equations of motion for the spins have the following form

$$\dot{\mathbf{S}}_k(t) = \mathbf{S}_k \times \frac{\partial E_{ex}}{\partial \mathbf{S}_k} \quad , \quad k = 1, \ldots, N-1. \tag{2.2.4}$$

For the energy in Eq. (2.2.1), we calculate

$$\frac{\partial E}{\partial \mathbf{S}_k} = -J \frac{\partial}{\partial \mathbf{S}_k} \sum_i^N \mathbf{S}_i \cdot \mathbf{S}_{i+1} = -J(\mathbf{S}_{k+1} + \mathbf{S}_{k-1}). \tag{2.2.5}$$

Finally, we substitute Eq. (2.2.4) and Eq. (2.2.5) and we obtain

$$\dot{\mathbf{S}}_k(t) = -J\mathbf{S}_k \times (\mathbf{S}_{k+1} + \mathbf{S}_{k-1}). \tag{2.2.6}$$

2.3 The magnetization vector

We suppose that all atoms in a specific material have a magnetic moment with the same magnitude, or that we can attribute to each lattice site in a solid material a magnetic moment with a certain constant magnitude. The magnetization properties of the material are defined by the atomic magnetic moments. In a ferromagnetic material the vector for the magnetic moment varies only slowly in space and it is then useful to treat the underlying material as a ferromagnetic continuum. That is, we may define the total magnetic moment in the unit volume of the material, or the density of magnetic moment $\mathbf{M}$. We define the magnetization as the density of magnetic moments

$$\mathbf{M} = \frac{\Delta\mu}{\Delta V}. \tag{2.3.1}$$

Where $\Delta\mu$ is the total magnetic moment in a volume element ΔV . The magnetization $\mathbf{M}$ has units (Ampere/meter) in SI.

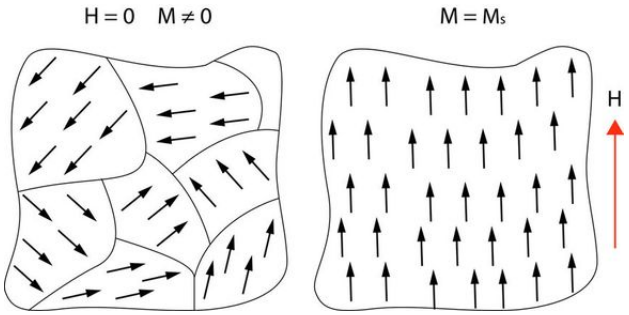

Figure 2.2: Magnetic domains.

The magnetic moment density M is called the magnetization vector. As it gives the local density of the magnetic moments it is a function of position and time, $M = M(r, t)$. As the magnetic moments of atoms are constant in magnitude the magnetization vector M is also considered to have a length which is constant . This is expressed as

$$\mathbf{M}^2 = M_s^2. \tag{2.3.2}$$

Where M_s is called the saturation magnetization. The saturation magnetization can easily be measured when a magnetic sample is fully magnetized (saturated) along a certain direction (e.g., by use of a strong magnetic field) .

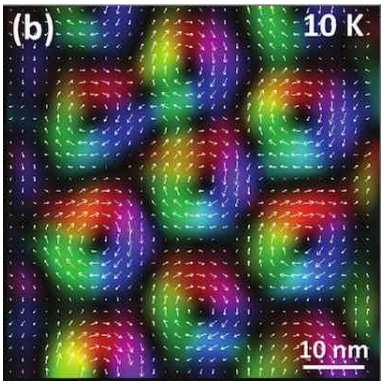

Figure 2.3: Magnetization configurations.[Source [Tonomura et al.]]

2.4 Continuum approximation

The form Eq. (2.2.1) of the exchange interaction for a discrete system of magnetic spins, these notes will only be concerned with a description of the continuum. In order to derive a model for the continuum Consider a small parameter ϵ (ϵ can be defined in different ways, for example, it may be the spacing between atoms or spins). Define

- A space variable $x = i\epsilon$
- A continuous field $\mathbf{S}(x)$ such that $\mathbf{S}(x) = \mathbf{S}_i$ at the position of each spin i

The continuous field $\mathbf{S}(x)$ is interpolating between the discrete spins (atoms) of the material.The advantage of defining a continuous spin field is that we can invoke a Taylor approximation. When ϵ is small, we may use the approximation

$$\mathbf{S}_{i\pm1} \approx \mathbf{S} \pm \epsilon\partial_x\mathbf{S} + \frac{\epsilon^2}{2}\partial_x^2\mathbf{S}, \qquad \mathbf{S}_i \to \mathbf{S}. \tag{2.4.1}$$

This assumes there is a continuous field $\mathbf{S}(x)$ and The spin changes little over neighbouring sites. Use the approximation (2.4.1) to obtain

$$\mathbf{S}_{i-1} + \mathbf{S}_{i+1} \approx \left(\mathbf{S} - \epsilon\partial_x\mathbf{S} + \frac{\epsilon^2}{2}\partial_x^2\mathbf{S}\right) + \left(\mathbf{S} + \epsilon\partial_x\mathbf{S} + \frac{\epsilon^2}{2}\partial_x^2\mathbf{S}\right) = 2\mathbf{S} + \epsilon^2\partial_x^2\mathbf{S}. \tag{2.4.2}$$

Substitute in the exchange energy

$$E_{ex} = -\frac{J}{2}\sum_i \mathbf{S}_i \cdot (\mathbf{S}_{i+1} + \mathbf{S}_{i-1}) = -J\sum\left(\mathbf{S}^2 + \frac{\epsilon^2}{2}\mathbf{S}\cdot\partial_x^2\mathbf{S}\right). \tag{2.4.3}$$

We may omit the constant $-Js^2$ (where $|\mathbf{S}_i| = s$) to have

$$E_{ex} \to -\frac{J}{2}\epsilon^2\sum \mathbf{S}\cdot\partial_x^2\mathbf{S}. \tag{2.4.4}$$

In the continuum approximation,using Eq. (2.4.4) the sum becomes an integral, if $\epsilon \to dx$

$$E_{ex} = -\frac{J}{2}\epsilon\int \mathbf{S}\cdot\partial_x^2\mathbf{S}\,dx.$$

We now change to the magnetisation $\mathbf{M} \sim \mathbf{S}$ and write $E_{ex} \sim -\int \mathbf{M}\cdot\partial_x^2\mathbf{M}\,dx$ and this gives by a partial integration

$$E_{ex} = \frac{A}{M_s^2}\int \partial_x\mathbf{M}\cdot\partial_x\mathbf{M}\,dx. \tag{2.4.5}$$

We have introduced the exchange constant A which has units of [Joule/meter], and the integration is extended over the volume of the magnetic material. The second form of the exchange energy is obtained from the first by a partial integration (divergence theorem).

The main property of a ferromagnet which is implied by the exchange energy (2.4.5) is that the magnetization should tend to be uniform, or, $\partial_x \mathbf{M} = 0$. On the other hand, the direction of the uniform magnetization is arbitrary, that is, the exchange energy term (2.4.5) is isotropic.

It will be very convenient for further calculations to rationalize the expression for the energy . First, it is natural to normalize $\mathbf{M}$, as well as all quantities with the same units, to the saturation magnetization M_s. We define the rationalized fields

$$\mathbf{m} = \frac{\mathbf{M}}{M_s}. \tag{2.4.6}$$

We further notice that the exchange term in the energy contains space derivatives, and therefore the ratio of the constant multiplying the exchange integral to would produce a natural length scale for the system. This motivates the definition of the exchange length

$$\ell_{ex} = \sqrt{\frac{2A}{M_s^2}}. \tag{2.4.7}$$

Substituting the definitions (2.4.6) in the energy (2.4.5) and measuring length in units of exchange length (i.e., substitute $x \to \ell_{ex} x$) , we obtain

$$E_{ex} = (M_s^2 \ell_{ex}^3) \frac{1}{2} \int \partial_x \mathbf{m} \cdot \partial_x \mathbf{m} \, dx. \tag{2.4.8}$$

We will assume in the following that the energy is measured in units of $(M_s^2 \ell_{ex}^3)$ so that the energy of the system is simply given by the term in the square brackets.Let us summarize here the rationalized form of the energy terms discussed in this section. The total energy of the exchange energy is

$$E_{ex} = \frac{1}{2} \int \partial_x \mathbf{m} \cdot \partial_x \mathbf{m} \, dx. \tag{2.4.9}$$

Example 2.1. We have for Permalloy $A = 1.3 \times 10^{-11}\,\mathrm{J/m}$, $M_s = 0.69 \times 10^6\,\mathrm{A/m}$. We calculate $\ell_{ex} = 6.59\,\mathrm{nm}$. □

We will consider (2.4.9) for the exchange energy. We have the Lagrangian density [AppendixA]

$$\mathcal{L} = \frac{1}{2} \partial_x \mathbf{m} \cdot \partial_x \mathbf{m}.$$

We have to consider the constraint $\mathbf{m}^2 = 1$. The constraint is imposed via a Lagrange multiplier $\lambda(x)$. We have to extremize the functional

$$L[\mathbf{m}] = \int dx \underbrace{\left[\frac{1}{2}\,\partial_x\mathbf{m}\cdot\partial_x\mathbf{m} + \frac{\lambda(x)}{2}(1-\mathbf{m}^2)\right]}_{\mathcal{L}}. \tag{2.4.10}$$

The functional L is minimized for $\mathbf{m}(x)$ that satisfies the Euler-Lagrange equation

$$-\frac{\delta L}{\delta \mathbf{m}} = 0 \Rightarrow \frac{d}{dx}\left(\frac{\partial \mathcal{L}}{\partial_x \mathbf{m}}\right) - \frac{\partial \mathcal{L}}{\partial \mathbf{m}} = 0. \tag{2.4.11}$$

We calculate and we remark

$$\partial_x^2\mathbf{m} + \lambda\mathbf{m} = 0. \tag{2.4.12}$$

In 3D, this is generalized as

$$\lambda\mathbf{m} + \nabla^2\mathbf{m} = 0. \tag{2.4.13}$$

We multiply the above by $\mathbf{m}$ in order to obtain the Lagrange multiplier

$$\mathbf{m}\cdot\nabla^2\mathbf{m} + \lambda\mathbf{m}\cdot\mathbf{m} = 0 \Rightarrow \lambda = -\mathbf{m}\cdot\nabla^2\mathbf{m}. \tag{2.4.14}$$

We use this to eliminate λ in the field Eq. (2.4.13)

$$\nabla^2\mathbf{m} - (\mathbf{m}\cdot\nabla^2\mathbf{m})\mathbf{m} = 0 \Rightarrow \mathbf{m}\times(\mathbf{m}\times\nabla^2\mathbf{m}) = 0. \tag{2.4.15}$$

The latter is equivalent to

$$\mathbf{m}\times\nabla^2\mathbf{m} = 0. \tag{2.4.16}$$

For the exchange energy, we have obtained the equation

$$\mathbf{m}\times\mathbf{f} = 0, \qquad \mathbf{f} = -\frac{\delta E_{ex}}{\delta \mathbf{m}} = \nabla^2\mathbf{m}. \tag{2.4.17}$$

This is generalized for any energy functional $E(\mathbf{m})$ and gives the Landau-Lifshitz equation

$$\mathbf{m}\times\mathbf{f} = 0, \qquad \mathbf{f} = -\frac{\delta E}{\delta \mathbf{m}}. \tag{2.4.18}$$

In that case (2.4.18) called the time-independent (or static) Landau-Lifshitz equation .

Chapter 3

Domain Walls

3.1 Domain Walls

A magnetic domain wall is an interface separating two magnetic domains. It is a transition layer between different magnetic moments and usually undergoes a rotation of 90° or 180°. A domain wall is a gradual reorientation of individual moments across a finite distance. The domain wall thickness depends on the anisotropy of the material, but on average spans across around 100–150 atoms.

The energy of a domain wall is simply the difference between the magnetic moments before and after the domain wall was created. This value is usually expressed as energy per unit wall area.

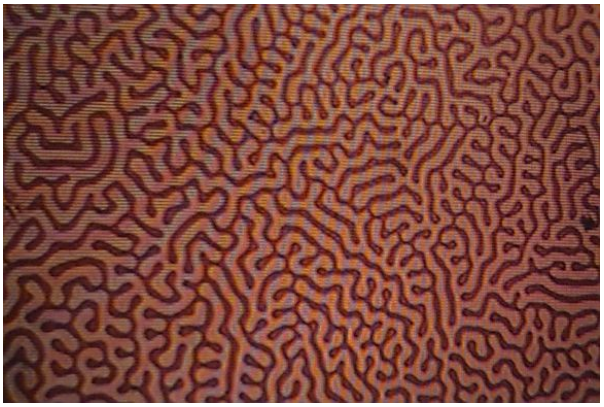

Figure 3.1: Domains in a ferromagnetic film. The magnetization points "up" in dark-coloured regions and "down" in light-coloured regions.

The width of the domain wall varies due to the two opposing energies that create it: the magnetocrystalline anisotropy energy and the exchange energy J_{ex}), both of which tend to be as low as possible so as to be in a more favorable energetic state. The anisotropy energy is lowest when the individual magnetic moments are aligned with the crystal lattice axes thus reducing the width of the domain wall. Conversely, the exchange energy is reduced when the magnetic moments are aligned parallel to each other and thus makes the wall thicker, due to the repulsion between them (where anti-parallel alignment would bring them closer, working to reduce the wall thickness). In

the end an equilibrium is reached between the two and the domain wall width is set as such.

An ideal domain wall would be fully independent of position , but the structures are not ideal and so get stuck on inclusion sites within the medium, also known as crystallographic defects. These include missing or different (foreign) atoms, oxides, insulators and even stresses within the crystal. This prevents the formation of domain walls and also inhibits their propagation through the medium. Thus a greater applied magnetic field is required to overcome these sites.

We have two types of walls bloch and neel

Case 1 : (Bloch Wall) A Bloch wall is a narrow transition region at the boundary between magnetic domains, over which the magnetization changes from its value in one domain to that in the next , named after the physicist Felix Bloch. In a Bloch domain wall, the magnetization rotates about the normal of the domain wall (in other words, the magnetization always points along the domain wall plane in a 3D system)

Bloch domain walls appear in bulk materials, i.e. when sizes of magnetic material are considerably larger than domain wall width (according to the width definition of Lilley). In this case energy of the demagnetization field does not impact the micromagnetic structure of wall. The mixed cases are possible as well when demagnetization field changes the magnetic domains (magnetization direction in domains) but not the domain walls.

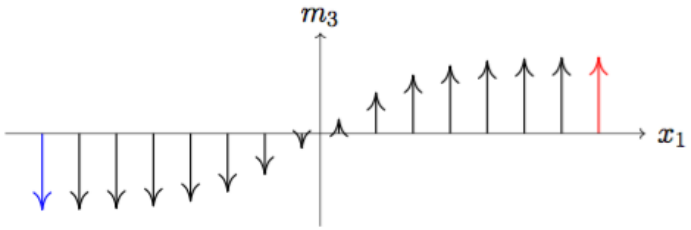

Figure 3.2: The magnetic configuration between domains turns from down to up gradually. [Source [6].]

Case 2 : (Neel Wall) A Néel wall is a narrow transition region between magnetic domains, named after the French physicist Louis Néel. In the Néel wall, the magnetization smoothly rotates from the direction of magnetization within the first domain to the direction of magnetization within the second. In contrast to Bloch walls, the magnetization rotates about a line that is orthogonal to the normal of the domain wall (in other words, it rotates such that it points out of the domain wall plane in a 3D system). It consists of a core with fast varying rotation (where the magnetization points nearly orthogonal to the two domains) and two tails where the rotation logarithmically decays . Néel walls are the common magnetic domain wall type in very thin films where the exchange length is very large compared to the thickness. Néel walls would spread across the whole volume if not for magnetic anisotropy .

3.2 Energy and equation of motion for a model with anisotropy

3.2.1 Easy-plane anisotropy

It is commonly seen that there are preferred directions in space for the orientation of magnetic moments, which depend on the crystal lattice of the material. We call this property the magnetocrystaline anisotropy or simply magnetic anisotropy. The simplest case is uniaxial magnetic anisotropy and it can be expressed by an energy term of the form

$$E_{\text{an}} = -g \sum_{i}^{N} S_{i,3}^2. \tag{3.2.1}$$

where g is the anisotropy constant . The continuum approximation,we change to the magnetisation $\mathbf{M} \sim \mathbf{S}$ and this gives

$$E_{an} = \frac{K}{M_s^2} \int (M_3)^2 \, dx. \quad \texttt{(Easy-plane anisotropy)} \tag{3.2.2}$$

where K is the anisotropy constant (Joule/meter^3) . If we assume $K > 0$, the energy term (3.2.2) disfavours the third component M_3 of the magnetization over the other two components (M_1, M_2) . Such an energy term gives rise to easy-plane anisotropy, that is, the magnetization vector prefers to lie in the xy-plane .

Substituting the definitions (2.4.5) , (2.4.6) , (2.4.7) and (3.2.2) and measuring length in units of exchange length (i.e., substitute $x \to \ell_{ex} x$) , we obtain

$$E = (M_s^2 \ell_{ex}^3) \left[\frac{1}{2} \int \partial_x \mathbf{m} \partial_x \mathbf{m} \, dx + \frac{k^2}{2} \int (m_3)^2 \, dx \right]. \tag{3.2.3}$$

The only constant remaining in the definition of the energy is multiplying the anisotropy term, it is called the quality factor

$$k = \sqrt{\frac{2K}{M_s^2}},$$

and measures the strength of the anisotropy relative to the magnetostatic term . Let us summarize here the rationalized form of the energy terms discussed in this section. The total energy is the sum of the exchange + anisotropy energy

$$E = E_{ex} + E_{an} = \frac{1}{2} \int \partial_x \mathbf{m} \cdot \partial_x \mathbf{m} \, dx + \frac{k^2}{2} \int m_3^2 \, dx. \tag{3.2.4}$$

We have the Lagrangian density Eq. (3.2.4) ,the variational derivative is (ϵ is the energy density, i.e., the integrand)

$$\mathbf{f} = -\frac{\delta E}{\delta \mathbf{m}} = \frac{d}{dx} \left(\frac{\partial \epsilon}{\partial (\partial_x \mathbf{m})} \right) - \frac{\partial \epsilon}{\partial \mathbf{m}} = \partial_x^2 \mathbf{m} - k^2 m_3 \hat{\mathbf{e}}_z.$$

The Landau-Lifshitz equation for exchange and easy-axis anisotropy is

$$\mathbf{m} \times \underbrace{\left(\nabla^2 \mathbf{m} - k^2 m_3 \hat{\mathbf{e}}_z \right)}_{\mathbf{f}} = 0. \tag{3.2.5}$$

3.2.2 Easy-axis anisotropy

We consinder the case K < 0 the M_3 component is favoured and we would thus call the above an easy-axis anisotropy term

$$E_{\text{an}} = g \sum_{i}^{N} [1 - S_{i,3}^2]. \tag{3.2.6}$$

where g is the anisotropy constant . The continuum approximation,we change to the magnetisation $\mathbf{M} \sim \mathbf{S}$ and this gives

$$E_{an} = \frac{K}{M_s^2} \int (M_s^2 - M_3^2)\, dx. \quad \texttt{(Easy-axis anisotropy)} \tag{3.2.7}$$

favours the states where $\mathbf{M}$ is fully aligned along the third axis, i.e., $M_3 = \pm M_s$ or $\mathbf{M} = (0, 0, \pm M_s)$.The minimum energy magnetisation configurations are $\mathbf{M}(x) = (0, 0, \pm M_s)$.

Substituting the definitions (2.4.5) , (2.4.6) , (2.4.7) and (3.2.7) and measuring length in units of exchange length (i.e., substitute $x \to \ell_{ex} x$) , we obtain

$$E = (M_s^2 \ell_{ex}^3) \left[\frac{1}{2} \int \partial_x \mathbf{m} \partial_x \mathbf{m}\, dx + \frac{k^2}{2} \int (1 - m_3^2)\, dx \right]. \tag{3.2.8}$$

The only constant remaining in the definition of the energy is multiplying the anisotropy term, it is called the quality factor

$$k = \sqrt{\frac{2K}{M_s^2}},$$

and measures the strength of the anisotropy relative to the magnetostatic term . Let us summarize here the rationalized form of the energy terms discussed in this section. The total energy is the sum of the exchange + anisotropy energy

$$E = E_{ex} + E_{an} = \frac{1}{2} \int \partial_x \mathbf{m} \cdot \partial_x \mathbf{m}\, dx + \frac{k^2}{2} \int (1 - m_3^2)\, dx. \tag{3.2.9}$$

We have the Lagrangian density Eq. (3.2.9) ,the variational derivative is (ϵ is the energy density, i.e., the integrand)

$$\mathbf{f} = -\frac{\delta E}{\delta \mathbf{m}} = \frac{d}{dx} \left(\frac{\partial \epsilon}{\partial (\partial_x \mathbf{m})} \right) - \frac{\partial \epsilon}{\partial \mathbf{m}} = \partial_x^2 \mathbf{m} + k^2 m_3 \hat{\mathbf{e}}_z.$$

The Landau-Lifshitz equation for exchange and easy-axis anisotropy is

$$\mathbf{m} \times \underbrace{\left(\nabla^2 \mathbf{m} + k^2 m_3 \hat{\mathbf{e}}_z \right)}_{\mathbf{f}} = 0. \tag{3.2.10}$$

3.3 Domain wall solution

In order to make more realistic models , we may consider adding an easy-axis anisotropy

$$\frac{\partial \mathbf{m}}{\partial t} = -\mathbf{m} \times (\nabla^2 \mathbf{m} + k^2 m_3 \hat{e_3}). \tag{3.3.1}$$

Where k is the parameter of anisotropy . The equation of motion in case of one-dimession has the following form

$$\frac{\partial \mathbf{m}}{\partial t} = -\mathbf{m} \times (\partial_x^2 \mathbf{m} + k^2 m_3 \hat{\mathbf{e}}_3). \tag{3.3.2}$$

Using spherical parametrisation of the magnetisation with the angles Θ, Φ

$$m_1 = \sin\Theta\cos\Phi, \quad m_2 = \sin\Theta\sin\Phi, \quad m_3 = \cos\Theta.$$

In a model with easy-axis anisotropy, we have two ground states, $\mathbf{m} = (0, 0, \pm 1)$, or $\Theta = 0, \pi$, that is, the north and south pole of the sphere.We look for a topological soliton connecting the north and the south pole. We confine ourselves to one space dimension $\mathbf{m} = \mathbf{m}(x)$ and We try the simplest possibility of a meridian on the Bloch sphere

$$\Theta = \Theta(x) \quad , \quad \Phi = \phi_0 : \text{const.}$$

Example 3.1. For $\phi_0 = \pi/2$, we have

$$m_1 = 0, \quad m_2(x) = \sin\Theta(x), \quad m_3(x) = \cos\Theta(x).$$

□

Consider exchange and easy-axis anisotropy (with parameter k^2). The Landau-Lifshitz equation is

$$\mathbf{m} \times \left(\mathbf{m}'' + k^2 m_3 \hat{\mathbf{e}}_z\right) = 0 \Rightarrow \begin{cases} m_2 m_3'' - m_3 m_2'' + k^2 m_2 m_3 = 0 \\ m_3 m_1'' - m_1 m_3'' - k^2 m_1 m_3 = 0 \\ m_1 m_2'' - m_2 m_1'' = 0\,. \end{cases}$$

Substitute the form for a Bloch wall $m_1 = 0,\ m_2 = \sin\Theta,\ m_3 = \cos\Theta$, whence only the first equation remains (the other two are trivially satisfied) . We calculate

$$m_2'' = -\sin\Theta\,\Theta'^2 + \cos\Theta\,\Theta'', \quad m_3'' = -\cos\Theta\,\Theta'^2 - \sin\Theta\,\Theta''.$$

The first equation gives

$$\Theta'' - k^2 \sin\Theta\cos\Theta = 0. \tag{3.3.3}$$

Multiply by $2\Theta'$

$$\left[(\Theta')^2 - k^2\sin^2\Theta\right]' = 0 \Rightarrow (\Theta')^2 - k^2\sin^2\Theta = C.$$

There are many solutions for this one-dimensional equation . We are only interested in localised solutions. We consider uniform domains for large $|x|$, therefore, we require $\Theta = 0, \pi$ and $\Theta' = 0$ at $x = \pm\infty$ .Applying the condition at $x \to \pm\infty$, we get the value of the constant $C = 0$ and we have

$$\Theta' = \pm k \sin\Theta. \tag{3.3.4}$$

The solution of the latter is

$$e^{\pm kx} = \pm \tan\left(\frac{\Theta}{2}\right).$$

For the plus signs . For $x \to -\infty$ we have $\Theta = 0$ (north pole) and for $x \to +\infty$ we have $\Theta = \pi$ (south pole) . The calculations for the derivation of the domain wall solution hold also for ϕ_0 nonzero,

$$m_1 = \sin\Theta\cos\phi_0, \quad m_2 = \sin\Theta\sin\phi_0, \quad m_3 = \cos\Theta.$$

Using trigonometric identities (for the half angle), we have the magnetisation

$$m_1 = \frac{1}{\cosh(kx)}\cos\phi_0, \quad m_2 = \frac{1}{\cosh(kx)}\sin\phi_0, \quad m_3 = \tanh(kx). \tag{3.3.5}$$

This result is valid for boundary conditions $\mathbf{m}(x = \pm\infty) = (0, 0, \pm 1)$. We get a different domain wall solution for every $0 \leq \phi_0 < 2\pi$. Within the model with exchange and uniaxial anisotropy, the energy is the same for all walls.

Example 3.2. Bloch wall (choose $\phi_0 = \pm\pi/2$)

$$m_1 = 0, \quad m_2 = \pm\frac{1}{\cosh(kx)}, \quad m_3 = \tanh(kx).$$

□

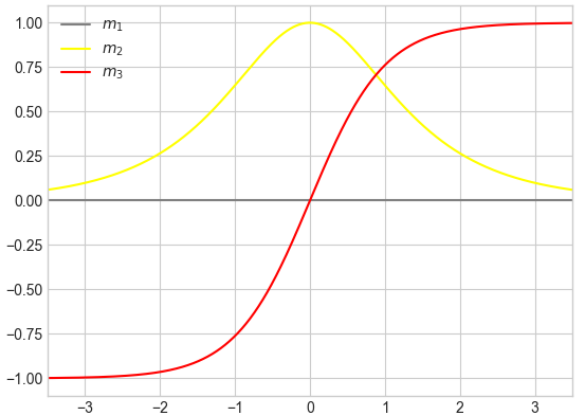

Figure 3.3: A Domain Wall as a solution of model with anisotropy.

Example 3.3. Neel wall (choose $\phi_0 = 0$)

$$m_1 = \pm\frac{1}{\cosh(kx)}, \quad m_2 = 0, \quad m_3 = \tanh(kx).$$

□

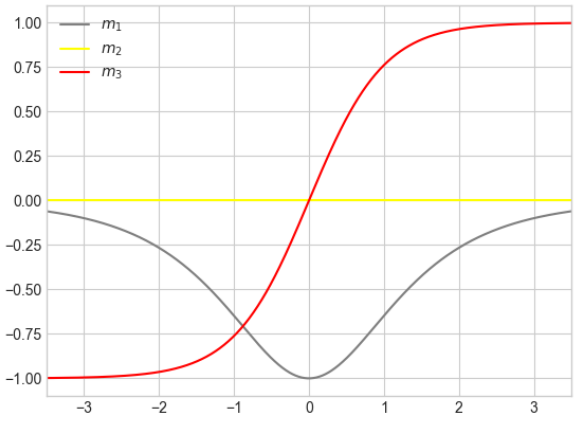

Figure 3.4: A Neel Wall as a solution of model with anisotropy.

3.4 Energy bound for domain walls

We consider Eq. (3.2.4) and we want find an energy bound of topological textures .so we noticed usining the spherical parametrization from previous chapter have the following computations

$$\partial_x \mathbf{m} \partial_x \mathbf{m} = (\partial_x \mathbf{m}_2)^2 + (\partial_x \mathbf{m}_3)^2 = \cos^2\Theta(\partial_x\Theta)^2 + \sin^2\Theta(\partial_x\Theta)^2 = (\partial_x\Theta)^2 = (\Theta')^2,$$

and also

$$1 - m_3^2 = 1 - \cos^2\Theta = \sin^2\Theta.$$

We consider the model with easy-axis anisotropy in one dimension. The energy Eq. (3.2.4) for a configuration $\Theta = \Theta(x)$ is

$$E = \frac{1}{2}\int (\Theta')^2\, dx + \frac{k^2}{2}\int \sin^2\Theta\, dx. \tag{3.4.1}$$

In order to derive a bound for the energy, we start with the following computations,

$$\frac{1}{2}(\Theta' \pm k\sin\Theta)^2 \geq 0 \Rightarrow \frac{1}{2}(\Theta')^2 + \frac{k^2}{2}\sin^2\Theta \pm k\Theta'\sin\Theta \geq 0. \tag{3.4.2}$$

We integrate on the plane and substitute in the energy (3.4.1) to obtain

$$E \geq \pm k\int_{-\infty}^{\infty} \sin\Theta\,\Theta'\, dx.$$

We now consider a domain wall with $\Theta(x \to -\infty) = 0$, $\Theta(x \to \infty) = \pi$ and we have

$$E \geq \pm k\int_0^{\pi} \sin\Theta\, d\Theta = \pm k[-\cos\Theta]_0^{\pi} = \pm 2k.$$

This implies the bound for the energy

$$E \geq 2k. \tag{3.4.3}$$

It would be good to stress that this bound is valid for topological configurations. The inequility is saturated when

$$\Theta' \pm k\sin\Theta = 0.$$

This equation coincides with Eq. (3.3.4) that has given the domain wall solutions (3.3.5).

3.5 Total magnetization

The simple model is invariant with respect to rotations around the z axis. Also, the out-of-plane magnetization is usually measured in experiments. These are the motivations for defining $\mathcal{M}$.It is reasonable that we study an integrated quantity, as is the total magnetization in the third direction

$$\mathcal{M} = \int m_3 \, dx. \tag{3.5.1}$$

We consider the conservative model with exchange and uniaxial anisotropy define Eq. (3.3.2) and calculate its time dependence

$$\frac{d\mathcal{M}}{dt} = \int \dot{m}_3 \, dx = -\int [\mathbf{m} \times (\mathbf{m}'' + k^2 m_3 \hat{e}_3)]_3 \, dx. \tag{3.5.2}$$

The second term has no z (third) component because $\mathbf{m} \times \hat{e}_3 \perp \hat{e}_3$, and

$$\int \boldsymbol{m} \times \mathbf{m}'' dx = \int (\mathbf{m} \times \mathbf{m}')' dx = [\mathbf{m} \times \mathbf{m}']_{-\infty}^{\infty} = 0. \tag{3.5.3}$$

We notice the total magnetisation is equal

$$\frac{d\mathcal{M}}{dt} = 0 \Rightarrow \mathcal{M} : \text{const.} \tag{3.5.4}$$

The total magnetisation is a conserved quantity for the above conservative model. Notice that the exchange and uniaxial anisotropies are symmetric with respect to rotations of the magnetisation around the third axis $\hat{e}_3$. By Noether's theorem, this gives conservation of the total magnetisation $\mathcal{M}$.

Chapter 4

Chiral Domain Wall

4.1 Dzyaloshinskii-Moriya Interaction

Chirality is a form of asymmetry of the system. If the atomic structure of a magnet lacks inversion symmetry we call them chiral magnets. The chirality expresses itself through the phase diagram which shows additional chiral phases.

In 1960 Dzyaloshinskii constructed a model to describe weak ferromagnetism . Based on symmetries he introduced an asymmetrical term which later on was dubbed the DzyaloshinskiiMoriya interaction. Moriya connected his name to this term when he found the mechanism behind this interaction is partly based on spin-orbit coupling . Without going into details we conclude that the Dzyaloshinskii-Moriya interaction is induced by a lack of inversion symmetry of the compound and a strong spin-orbit coupling.

An example of a compound that lacks inversion symmetry is MnSi (manganese silicide), as depicted schematically in Fig. 4.1. In the figure we see that inversion symmetry is broken in a unit cell. Aside from a lack of inversion symmetry, MnSi has a strong spin- orbit coupling. This is due to several microscopic processes, which we will not go into.

Figure 4.1: Schematic figure of the atomic structure of MnSi. The circles represent atoms and the dashed lines depict the boundaries of a unit cell. We see that this structure lacks inversion symmetry in a unit cell.[Source [7].]

Inversion symmetry can be broken in different directions leading to a different induced DM interaction. In practice this means that the magnetization is different. We consider an example of just two spins here, however in the coming sections of this thesis we consider a bigger system. The DM interaction for two spins has the following form

$$\mathcal{H}_{DM} = -D_{12} \cdot (\mathbf{S}_1 \times \mathbf{S}_2) \tag{4.1.1}$$

In this expression $\mathbf{S}_1$ and $\mathbf{S}_2$ are the atomic spins . In Fig. 4.2 there is a DM interaction emerging from the interplay of two atomic spins with a neighboring atom having a large spin-orbit coupling in a thin film. The resulting DM interaction points outwards from the plane of the atoms. The same mechanism is responsible for the interfacial DM interaction between a ferromagnetic thin layer and a non-magnetic layer with a large spin-orbit coupling. Here, at the interface between the two layers, the triangle mechanism produces a DM interaction for the interfacial spins S1 and S2. The DM interaction vector, D_{12}, is perpendicular to the triangle.Starting with a ferromagnetic state where all spin are alligned: $\mathbf{S}_1||\mathbf{S}_2$, we then assume a strong spin-orbit coupling present that induces a DM interaction. The resulting magnetic structure depends on the direction of the D-vector, which in turn depends on the way which the symmetry in the compound is broken. Different helicities are obtained for different DM interactions.

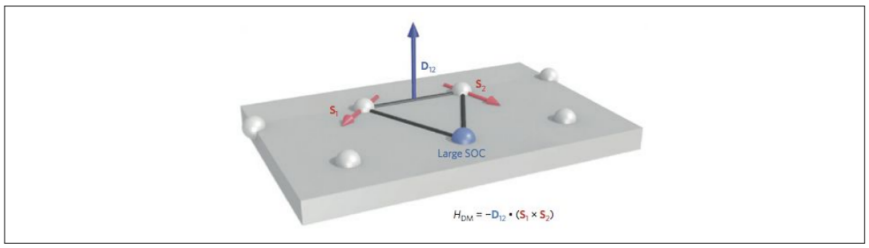

Figure 4.2: Schematic explanation of the interfacial DM interaction for two spins.[Source [7].]

4.2 Energy and equation of motion

We will assume a ferromagnet with exchange, an easy-axis anisotropy, and a DMI. We will study configurations where the magnetization is varying in only one space direction, that is, we assume $\mathbf{m} = \mathbf{m}(x,t)$. The energy of such a system is

$$E(\mathbf{m}) = \frac{1}{2}\int [(\partial_x \mathbf{m})^2 + k^2(1-m_3^2) + 2\lambda(\mathbf{m}\times\partial_x\mathbf{m})\cdot\hat{e}_1]\,dx. \tag{4.2.1}$$

where $\hat{e}_1$ is the unit vector for the magnetization in the x direction. We measure distance in units of exchange length $\ell_{ex} = \sqrt{2A/\mu_0 M_s^2}$ where A is the exchange constant. There are two length scales in the model $\ell_w = \sqrt{A/K}$, where K is the anisotropy constant, and $D = 2A\,|D|$, where D is the DMI constant. The dimensionless parameters appearing in the energy (4.2.1) are $k^2 = 2K\ (\mu_0 M_s^2) = (\ell_{ex}/\ell_w)^2$, and $\lambda = \ell_{ex}/\ell_D$. We will consider $\lambda > 0$; the case $\lambda < 0$ corresponds to the transformation $x \to -x$. The general form of the DM term is given in terms of Lifshitz invariants

$$\mathcal{L}_{ij} = (\mathbf{m}\times\partial_i\mathbf{m})_j. \tag{4.2.2}$$

In the energy (4.2.1) we have only kept the Lifshitz invariant $\mathcal{L}_{11}$ in the $\hat{e}_1$ direction corresponding to cubic DMI given by $\mathbf{m}\cdot(\nabla\times\mathbf{m})$. Replacing $\mathcal{L}_{11}$ by $\mathcal{L}_{12}$ (interfacial DMI) or a linear combination of both yields a model that is mathematically equivalent modulo a rigid rotation around the $\hat{e}_3$ axis.The effective field entering (4.2.4) is obtained by varying the energy,

$$\mathbf{f} = \frac{\delta E}{\delta \mathbf{m}} = \partial_x^2\mathbf{m} + k^2 m_3\hat{e}_3 - 2\lambda\hat{e}_1\times\partial_x\mathbf{m}. \tag{4.2.3}$$

he uniform (ferromagnetic) states $\mathbf{m} = (0, 0\pm1)$ are the simplest time-independent (static) solutions of the LL equation

$$\frac{\partial\mathbf{m}}{\partial t} = -\mathbf{m}\times\mathbf{f} = 0. \tag{4.2.4}$$

4.3 Energy bound for chiral domain walls

We consider the Eq. (4.2.1) of energy and we want find an energy bound of topological textures . So we noticed that

$$\partial_x \mathbf{m} \partial_x \mathbf{m} = (\partial_x \mathbf{m}_2)^2 + (\partial_x \mathbf{m}_3)^2 = \cos^2\Theta(\partial_x\Theta)^2 + \sin^2\Theta(\partial_x\Theta)^2 = (\partial_x\Theta)^2 = (\Theta')^2.$$

and also using the trigonometric identities

$$1 - m_3^2 = 1 - \cos^2\Theta = \sin^2\Theta.$$

Moreover we have the following computations for chiral term

$$\hat{e}_x \cdot (\mathbf{m} \times \partial_x \mathbf{m}) = m_2 \partial_x m_3 - m_3 \partial_x m_2 =$$
$$\sin\Theta(x)(-\sin\Theta(x))\partial_x\Theta(x) - \cos\Theta(\cos\Theta)\partial_x\Theta(x) = -\partial_x\Theta(x) = \Theta'.$$

We write again energy form and noticed

$$E = E_{ex} + E_{an} + E_{DM} =$$

$$\frac{1}{2}\int \partial_x \mathbf{m} \partial_x \mathbf{m}\, dx + \frac{k^2}{2}\int (1 - m_3^2)\, dx - \lambda \int \hat{e}_x \cdot (\mathbf{m} \times \partial_x \mathbf{m}) =$$
$$\frac{1}{2}\int (\Theta')^2\, dx + \frac{k^2}{2}\int \sin^2\Theta\, dx + \lambda \int \Theta'\, dx.$$

Make the following computations

$$\frac{1}{2}(\Theta' \pm q\sin\Theta)^2 \geq 0 \Rightarrow \frac{1}{2}(\Theta')^2 + \frac{k^2}{2}\sin^2\Theta \pm k\Theta'\sin\Theta \geq 0 \Rightarrow$$
$$\frac{1}{2}(\Theta')^2 + \frac{k^2}{2}\sin^2\Theta + \lambda\Theta' \geq \pm k\Theta'\sin\Theta + \lambda\Theta',$$

We integrate over the plane and get

$$E \geq \pm \int k\Theta'\sin\Theta \quad dx + \lambda \int \Theta' \quad dx \Rightarrow E \geq \pm k \int d(\cos\Theta) + \lambda \int_{\pi}^{0} d\Theta \Rightarrow$$
$$E \geq 2k - \lambda\pi. \tag{4.3.1}$$

Finally define Eq. (4.3.1) we have

$$E \geq 0 \Rightarrow \lambda \leq \frac{2k}{\pi} \quad \text{and} \quad E < 0 \Rightarrow \lambda > \frac{2k}{\pi}. \tag{4.3.2}$$

Usually we choose anisotropy parameter $k = 1$, so in that case the lowest energy (ground) state is the spiral for $\lambda > 2/\pi$ and the ferromagnetic state for $\lambda < 2/\pi$.

4.4 Traveling domain walls

Many interesting phenomena in magnetic materials refer to switching of the magnetization of domains. One way to achieve this is to shift the domain wall between two domains of opposite magnetization. This way one of the domains expands at the expense of the other. This brings forward the problem of a propagating domain wall. Suppose two domains of opposite magnetization separated e.g., $\boldsymbol{m} = (0, 0, 1)$ and $\boldsymbol{m} = (0, 0, -1)$ respectively. Expanding the one domain is tantamount to moving the domain wall to the direction of the other domain.

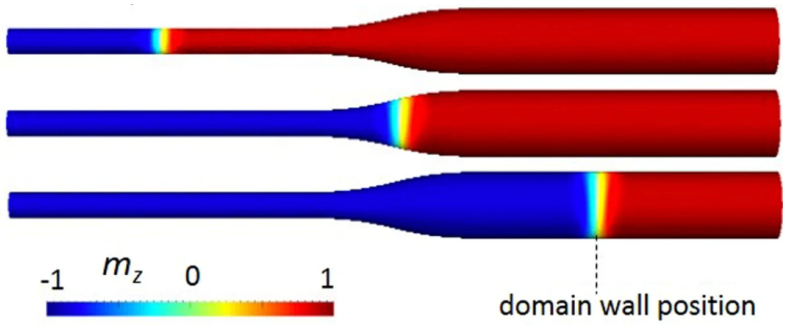

Figure 4.3: ail-to-tail domain wall displacement under the applied magnetic field. The color scale bar indicates the longitudinal magnetization m_z. [Source [8].]

then we may expect that expansion of the domain along the direction of the field may proceed through motion of the domain wall . We will be looking for a propagating wall of the special form

$$\mathbf{m} = \mathbf{m}(x - ut), \tag{4.4.1}$$

where u is a constant velocity for the domain wall.We consider a model including the Dzyaloshinskii-Moriya interaction define by Eq. (4.2.4), (4.2.3) . Let us recall that a Bloch wall is a static solution of the model (this is because $\mathbf{m} \times (\hat{e}_x \times \mathbf{m}') = -m_1 \mathbf{m}'$ and thus the DM term vanishes for a Bloch wall).The time dependence of the total magnetisation is

$$\frac{d\mathcal{M}}{dt} = \int \dot{m}_3 \, dx = -\int [\mathbf{m} \times (\mathbf{m}'' + k^2 \, m_3 \hat{e}_3 - 2\lambda \, \hat{e}_1 \times \boldsymbol{m}')]_3 \, dx. \tag{4.4.2}$$

The first two terms give zero and the third term gives

$$\frac{d\mathcal{M}}{dt} = -2\lambda \int_{-\infty}^{\infty} m_1 m_3' \, dx. \tag{4.4.3}$$

More generally,

- $\mathcal{M}$ is conserved when $\lambda = 0$ because exchange and anisotropy are invariant with respect to rotations around $\hat{e}_z$.
- The DM interaction breaks this symmetry, the associated conservation law is not valid, thus allowing for the possibility of propagating domain walls.
- A propagating wall should develop a nonzero m_1 component (tilting).

Let λ/k be sufficiently small. Then, there is a neighbourhood N of $\frac{\pi}{2}$, such that for $\varphi_0 \in N$ there is a strictly increasing domain wall solution of the equations. The domain wall velocity is $u \neq 0$ if $\varphi_0 \neq \pi/2$.Numerically found traveling domain walls have velocities in the range [9]

$$0 < u < 0.78.$$

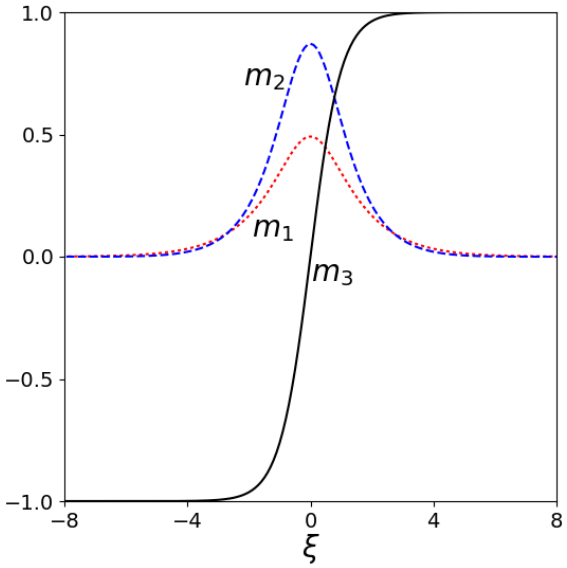

Figure 4.4: The three components of the magnetization for a chiral domain wall with velocity $u = 0.40$ traveling to the right,for parameter values are $k = 1,\ \lambda = 0.5$.[Source[9].]

Chapter 5

Skyrmions in the exchange model

5.1 BP Skyrmions

We consider a fully isotropic ferromagnet in two space dimensions, $\boldsymbol{m} = \boldsymbol{m}(x, y, t)$, thus we have the model that contains only the exchange interaction

$$\frac{\partial}{\partial t}\mathbf{m} = -\mathbf{m} \times \nabla^2 \mathbf{m}. \tag{5.1.1}$$

Our goal now is to find explicit solutions of the static Landau-Lifshitz equation in the case of magnetic films . It is convenient to map the magnetization defined on the Bloch sphere, to a complex function $u = u(z)$, with $z = x + iy$. The stereographic projection of a point on the sphere $\mathbf{m} = (\sin\theta\cos\phi, \sin\theta\sin\phi, \cos\theta)$ to the complex plane is given by

$$u = \frac{m_x + i m_y}{1 + m_z} = \tan\frac{\theta}{2} e^{i\phi}. \tag{5.1.2}$$

Eq. (5.1.2) is inverted to give

$$m_x = \frac{u + \overline{u}}{1 + u\overline{u}} \quad , \quad m_y = \frac{1}{i}\frac{u - \overline{u}}{1 + u\overline{u}} \quad , \quad m_z = \frac{1 - |u|^2}{1 + |u|^2}.$$

where the over bar represents complex conjugation.

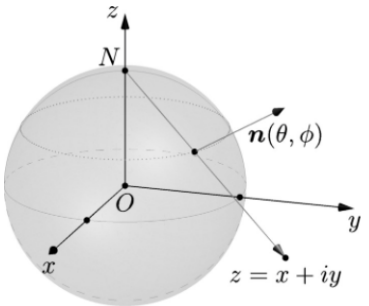

Figure 5.1: Stereographic Projection in a Complex Plane.

The static Landau-Lifshitz equation in the new function u, becomes

$$0 = i\partial_t u = -\partial\overline{\partial}u + 2\frac{2\overline{u}}{1+|u|^2}\partial u\overline{\partial}u, \tag{5.1.3}$$

where $\partial = \partial/\partial_z = (\partial/\partial_x - i\partial/\partial_y)/2$. One immediately observes that any harmonic function is a stationary solution [10].

$$\overline{\partial}u(z) = 0 \quad \texttt{or} \quad \partial u(z) = 0. \tag{5.1.4}$$

General every complex function $u = u(z)$ where $z = x+iy$ and $u(z) = u_1(x,y)+iu_2(x,y)$ which satisfied the cauchy - Riemann equation $\partial_1 u_1 = \pm\partial_2 u_2,\ \partial_2 u_1 = \mp\partial_1 u_2$ is a solution of exchange model. For example, a solutions of this form are

$$u = \alpha z,\ \alpha z^2,\ \frac{\alpha}{z},\ \frac{\alpha}{\overline{z}},\ \alpha\overline{z}, \ldots \qquad \alpha \in \mathbb{R}^+$$

where α is a constant. Any rational polynomial of z is a solution and also any rational polynomial of $\bar{z}$ is a solution.

Example 5.1. We consider

$$u = \alpha z.$$

This gives the magnetization components

$$m_x = \frac{2\alpha x}{1+\alpha^2(x^2+y^2)}, \quad m_y = \frac{2\alpha y}{1+\alpha^2(x^2+y^2)}, \quad m_z = \frac{1-\alpha^2(x^2+y^2)}{1+\alpha^2(x^2+y^2)}.$$

Fig. 5.2 shows the skyrmion configuration.

□

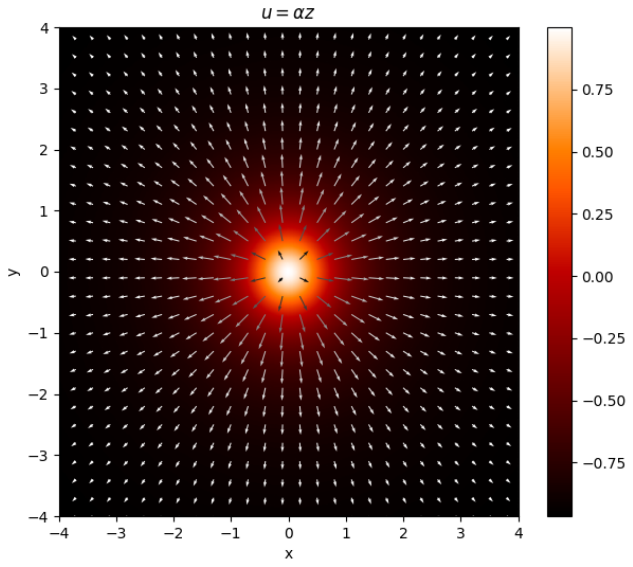

Figure 5.2: A BP skyrmion obtained for $u = \alpha z$ with the choice $\alpha = 1.33$. The vectors shows the projection of $\mathbf{m}$ on the plane, i.e., (m_1, m_2). The 3rd component of the magnetization m_3 is represented by the color code as shown on the right of the figure.

Example 5.2. We consider

$$u = \frac{\alpha}{\bar{z}}.$$

This gives the magnetization components

$$m_x = \frac{2\alpha x}{1+\alpha^2(x^2+y^2)}, m_y = \frac{2\alpha y}{1+\alpha^2(x^2+y^2)}, m_z = \frac{1-\alpha^2(x^2+y^2)}{1+\alpha^2(x^2+y^2)}.$$

Fig. 5.3 shows the skyrmion configuration. □

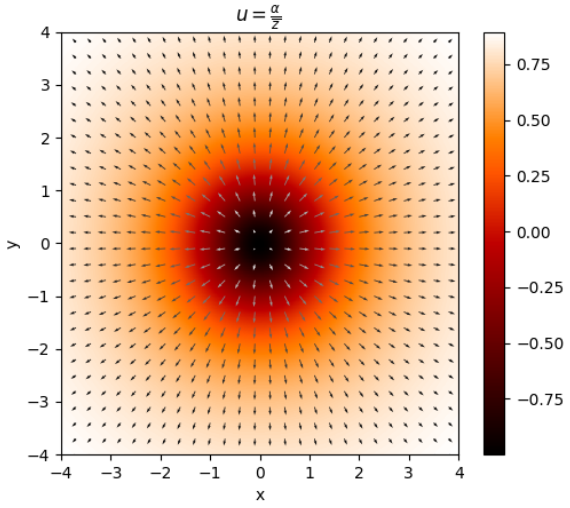

Figure 5.3: A BP Skyrmion obtained for $u = \alpha/\bar{z}$ with the choice $\alpha = 1.33$. The vectors and color code are as in Fig. 5.2.

Example 5.3. We consider

$$u = \alpha z^2.$$

This gives the magnetization components

$$m_x = \frac{2\alpha(x^2-y^2)}{1+\alpha^2(x^2+y^2)^2}, \quad m_y = \frac{4\alpha xy}{1+\alpha^2(x^2+y^2)^2}, \quad m_z = \frac{1-\alpha^2(x^2+y^2)^2}{1+\alpha^2(x^2+y^2)^2}$$

Fig. 5.4 shows the skyrmion configuration. □

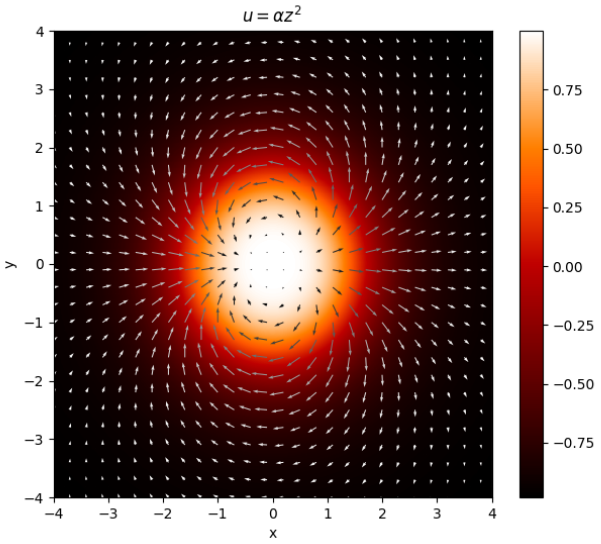

Figure 5.4: A BP Skyrmion $u = \alpha z^2$ with the choice $\alpha = 0.33$. The vectors and color code are as in Fig. 5.2.

Example 5.4. We consider

$$u = \alpha \overline{z}.$$

This gives the magnetization components

$$m_x = \frac{2\alpha x}{1+\alpha^2(x^2+y^2)}, \quad m_y = \frac{-2\alpha y}{1+\alpha^2(x^2+y^2)}, \quad m_z = \frac{-1+\alpha^2(x^2+y^2)}{1+\alpha^2(x^2+y^2)}.$$

Fig. 5.5 shows the skyrmion configuration. □

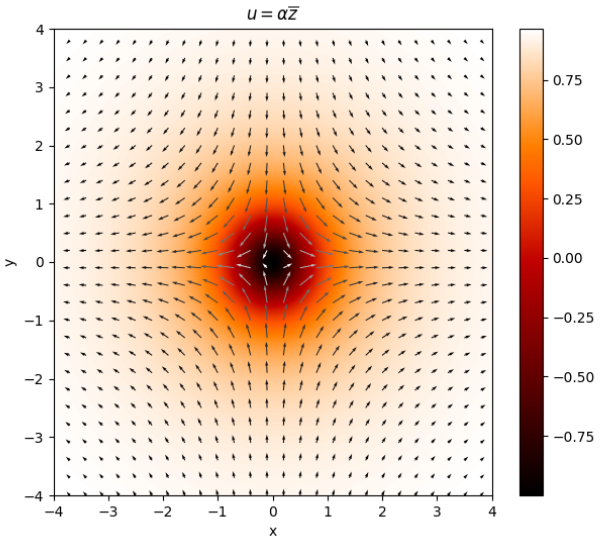

Figure 5.5: A BP skyrmion with $u = \alpha \overline{z}$ with the choice $\alpha = 1.33$. The vectors and color code are as in Fig. 5.2.

Example 5.5. A more complicated form could be (Noticed this form satisfied the Cauchy-Riemann equations)

$$u = \frac{\alpha i}{\overline{z} + d/2} - \frac{\alpha i}{\overline{z} - d/2}.$$

□

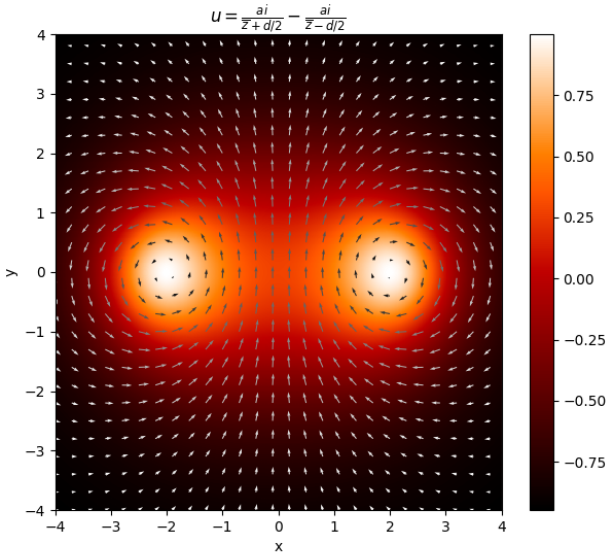

Figure 5.6: A BP Skyrmion which called Biskyrmion.

The exchange model possesses the following simple symmetries.

- The energy is invariant under scale transformations. Thus, the BP solutions have the same energy under the transformation $z \to az$. For example, the BP solution in Fig. 5.3 has the same energy for any value of the constant a.
- The energy is invariant under global rotations of the magnetization vector. For example the BP skyrmion Fig. 5.3 has the same energy if we set $a \to a^{i\phi}$ for any angle ϕ.
- More generally, the model possesses conformal invariance. We could rotate all vectors by any angle and obtain a further skyrmion (solution of the equations). More general transformations can be applied and obtain more skyrmion solutions (due to the conformal invariance of the model).

Example 5.6. We consinder

$$u = \alpha z.$$

But this time we choose $\alpha = i$ and notice □

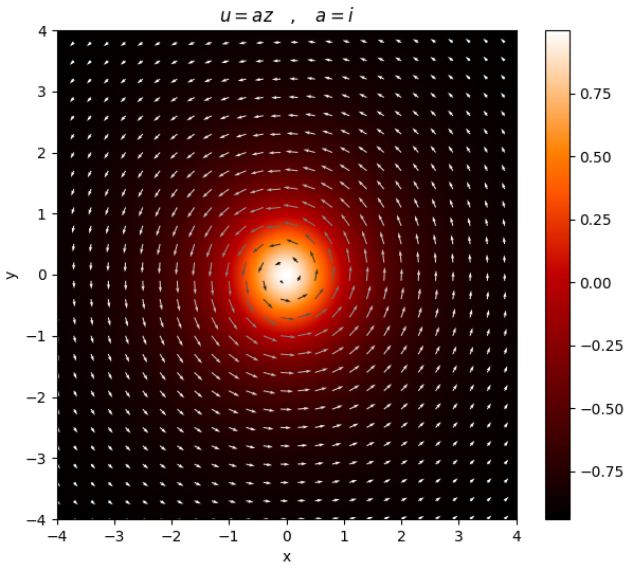

Figure 5.7: A BP skyrmion with $a = i$. All vectors are rotated by $\pi/2$.

5.2 Skyrmion Number for Axially Symmetry Configuration

From (1.2.1) we known the formula of Skyrmion number , so we rewrite in the following form

$$Q = \frac{1}{4\pi}\int q d^2x \quad , \quad q = \frac{1}{2}\epsilon_{\mu\nu}\mathbf{m}(\partial_\nu \mathbf{m} \times \partial_\mu \mathbf{m}). \tag{5.2.1}$$

The indexes μ, ν takes values $\mu, \nu = 1, 2, 3$ and we employ the Einstein summation convention (the repeated indexes μ, ν are summed over its three values) . We now focus on axially symmetric skyrmion configurations. These are conveniently described in terms of the standard spherical parametrisation for the magnetization given by

$$m_1 = \sin\Theta\cos\Phi \quad , \quad m_2 = \sin\Theta\sin\Phi \quad , \quad m_3 = \cos\Theta. \tag{5.2.2}$$

using the ansatz

$$\Theta = \theta(\rho) \quad , \quad \Phi = \phi + \pi/2, \tag{5.2.3}$$

where (ρ, ϕ) are polar coordinates. we could write the magnetization vector $\mathbf{m} = (m_1, m_2, m_3)$, with the following general expression

$$m_1 + im_2 = [m_\rho(\rho) + im_\phi(\rho)]e^{i(\phi+\pi/2)} \quad , \quad m_3 = m_z(\rho) \tag{5.2.4}$$

where m_ρ is the radial, m_ϕ is the azimuthal and m_z is the longitudinal coordinate of magnetization , with the following relation for m_ρ, m_ϕ, m_z

$$m_\rho^2 + m_\phi^2 + m_z^2 = 1. \tag{5.2.5}$$

It is very important to find a general formula for the Skyrme number characterized by the above structure. So we should express the topological density q as

$$q = (\partial_2\mathbf{m} \times \partial_1\mathbf{m}) \cdot \mathbf{m} = \frac{1}{\rho}(\partial_\phi\mathbf{m} \times \partial_\rho\mathbf{m}) \cdot \mathbf{m}. \tag{5.2.6}$$

For an axially symmetric configuration defined from Eq (5.2.1) we take the following formula

$$q = \frac{1}{\rho}[(m_1\partial_\phi m_2 - m_2\partial_\phi m_1)\partial_\rho m_3 + (\partial_\phi m_1\partial_\rho m_2 - \partial_\phi m_2\partial_\rho m_2)m_3]. \tag{5.2.7}$$

Using (5.2.4) and (5.2.7) we have the following computations

$$m_1\partial_\phi m_2 - m_2\partial_\phi m_1 = (m_\rho\sin\phi + m_\phi\cos\phi)^2 + (m_\phi\sin\phi - m_\rho\cos\phi)^2 = m_\rho^2 + m_\phi^2 \tag{5.2.8}$$

$$\partial_\phi m_1\partial_\rho m_2 - \partial_\phi m_2\partial_\rho m_2 = -(m_\rho\partial_\rho m_\rho + m_\phi\partial_\phi m_\phi) = m_z\partial_\phi m_z. \tag{5.2.9}$$

Finally the topological destiny reduces to

$$q = \frac{1}{\rho}((m_\rho^2 + m_\phi^2)\partial_\rho m_z + m_z^2\partial_\phi m_z) = \frac{1}{\rho}\,\partial_\rho m_z(\rho). \tag{5.2.10}$$

The topological number is

$$Q = \frac{1}{4\pi}\int q\,(2\pi\,\rho d\rho) = \frac{1}{2}\int_0^\infty \partial_\rho m_z\, d\rho = \frac{1}{2}[m_z(\rho\to\infty) - m_z(\rho=0)], \tag{5.2.11}$$

where $m_z = \cos\theta = m_z(\rho)$ is the third component of magnetization. Thus, if Eq. (5.2.11) is solved with boundary conditions $\Theta(\rho=0)=\pi$ and $\Theta(\rho\to\infty)=0$, it leads to a static skyrmion with $Q=1$.

Example 5.7. Let us consider Example 5.2 This is written using polar coordinates as

$$z = \rho e^{i\phi} \quad , \quad \bar{z} = \rho e^{-i\phi},$$
$$u = \frac{m_1 + i m_2}{1+m_3} = \frac{a}{\rho}\, e^{i\phi}.$$

□

If we assume $\alpha \in \mathbb{R}$, we have the magnetisation components

$$m_\rho = \frac{u+\bar{u}}{1+u\bar{u}} = \frac{2a\rho}{\rho^2+a^2}\cos\phi,$$
$$m_\phi = \frac{1}{i}\frac{u-\bar{u}}{1+u\bar{u}} = \frac{2a\rho}{\rho^2+a^2}\sin\phi,$$
$$m_z = \frac{1-u\bar{u}}{1+u\bar{u}} = \frac{\rho^2-a^2}{\rho^2+a^2}.$$

We note that

$$m_z(\rho=0) = -1,\ m_z(\rho\to\infty) = 1,$$

and the skyrmion number is

$$Q = \frac{1}{2}[m_z(\rho\to\infty) - m_z(\rho=0)] = 1 \quad \leftarrow \quad \texttt{BP Skyrmion (Q = 1)}\ .$$

Example 5.8. Let us consider Example 5.4 This is written using polar coordinates as

$$z = \rho e^{i\phi} \quad , \quad \bar{z} = \rho e^{-i\phi},$$
$$u = \frac{m_1 + i m_2}{1+m_3} = \alpha\rho e^{-i\phi},$$

□

Inverting this we have the magnetisation components (assume $\alpha \in \mathbb{R}$)

$$m_\rho = \frac{2\alpha x}{1+\alpha^2(x^2+y^2)},$$
$$m_\phi = \frac{-2\alpha y}{1+\alpha^2(x^2+y^2)},$$
$$m_z = \frac{-1+\alpha^2(x^2+y^2)}{1+\alpha^2(x^2+y^2)}.$$

So we note that

$$m_z(\rho = 0) = 1,\ m_z(\rho \to \infty) = -1.$$

$$Q = \frac{1}{2}[m_3(\rho \to \infty) - m_3(\rho = 0)] = -1 \quad \leftarrow \quad \texttt{BP Anti-Skyrmion (Q = -1)}\ .$$

Example 5.9. Let us consider Example 5.5 This is written using polar coordinates as

$$z = \rho e^{i\phi} \quad , \quad \bar{z} = \rho e^{-i\phi} \quad \texttt{(In polar coordinates)},$$

$$u = \frac{ai}{\bar{z} + d/2} - \frac{ai}{\bar{z} - d/2} \Rightarrow u = \frac{-iad}{\bar{z}^2 - (d/2)^2}.$$

□

We assume we are in a centrosymmetric material , so in that case we have

$$u = -2adi\frac{1}{\bar{z}^2} \Rightarrow u = \frac{m_1 + im_2}{1 + m_3} = -2adie^{i2\phi}.$$

Inverting this we have the magnetisation components (assume $\alpha \in \mathbb{R}$)

$$m_z = 2\frac{1 - u\bar{u}}{1 + u\bar{u}} = 2\frac{\rho^4 + a^2d^2}{\rho^4 - a^2d^2},$$

we note that

$$m_3(\rho = 0) = -2,\ m_3(\rho \to \infty) = 2.$$

In that case the skyrmion number gives

$$Q = \frac{1}{2}[m_z(\rho \to \infty) - m_z(\rho = 0)] = 2 \quad \texttt{Biskyrmion (Q = 2)}.$$

5.3 Energy bound for skyrmions

An energy bound for topological textures can be obtained if we start from the identity

$$(\partial_x \mathbf{m} \pm \mathbf{m} \times \partial_y \mathbf{m})^2 + (\partial_y \mathbf{m} \pm \mathbf{m} \times \partial_x \mathbf{m})^2 \geq 0. \tag{5.3.1}$$

Using a triple product identity, we have

$$(\partial_x \mathbf{m} \pm \mathbf{m} \times \partial_y \mathbf{m})^2 = (\partial_x \mathbf{m})^2 + (\partial_y \mathbf{m})^2 \pm 2\mathbf{m} \cdot (\partial_x \mathbf{m} \times \partial_y \mathbf{m}). \tag{5.3.2}$$

Similarly, we obtain

$$(\partial_y \mathbf{m} \pm \mathbf{m} \times \partial_x \mathbf{m})^2 = (\partial_x \mathbf{m})^2 + (\partial_y \mathbf{m})^2 \pm 2\mathbf{m} \cdot (\partial_x \mathbf{m} \times \partial_y \mathbf{m}). \tag{5.3.3}$$

We add the formulas (5.3.2) and (5.3.3) and we obtain

$$(\partial_x \mathbf{m} \pm \mathbf{m} \times \partial_y \mathbf{m})^2 + (\partial_y \mathbf{m} \pm \mathbf{m} \times \partial_x \mathbf{m})^2 = 2[(\partial_x \mathbf{m})^2 + (\partial_y \mathbf{m})^2] + 4q,$$

where q is called the topological density. We integrate over the plane and use Eq. (5.3.1) to obtain

$$2\int [(\partial_x \mathbf{m})^2 + (\partial_y \mathbf{m})^2] dxdy \pm 4 \int q dxdy \geq 0 \Rightarrow 4E \pm 16\pi Q \geq 0 \Rightarrow E \geq 4\pi |Q|. \tag{5.3.4}$$

The skyrmion number Q is integer-valued $(Q = 0, \pm 1, \pm 2, \dots)$ for all magnetic configurations such that $\mathbf{m} = (0, 0, \pm 1)$ at spatial infinity.

Example 5.10. For a skyrmion with $Q = 1$ (5.3.4) gives □

$$E = E_{ex} \geq 4\pi. \tag{5.3.5}$$

So for a skyrmion with $Q = 1$ energy can't be lower that $E_{ex} = 4\pi$.

5.4 A virial relation

Consider the model with exchange and easy-axis anisotropy energy in three space dimensions (3D)

$$E = E_{\rm ex} + E_{\rm an} = -J\sum_{i=1}^{N-1} \mathbf{S}_i \cdot \mathbf{S}_{i+1} + g\sum_{i=1}^{N}[1 - S_{i,3}^2]. \tag{5.4.1}$$

The continuum approximation using Eq. (2.4.5) and Eq. (3.2.7) gives

$$E = \frac{A}{M_s^2}\int \partial_\mu \mathbf{M} \cdot \partial_\mu \mathbf{M}\, d^3x + \frac{K}{M_s^2}\int (M_s^2 - M_3^2)\, d^3x. \tag{5.4.2}$$

Where $\mu = 1, 2, 3$ and $\partial_1 = \partial_x, \partial_2 = \partial_y, \partial_3 = \partial_z$. The variable $\mathbf{M}$ can be normalised to have unit length

$$\mathbf{m} = \frac{\mathbf{M}}{M_s}, \qquad \mathbf{m}^2 = 1.$$

The energy is

$$E = A\int \partial_\mu \mathbf{m} \cdot \partial_\mu \mathbf{m}\, d^3x + K\int (1 - m_3^2)\, d^3x. \tag{5.4.3}$$

Consider the dimensions of the parameters $[A], [K]$.

- From the first term $[E] = [A][L]$ ($[E], [L]$ indicate dimensions of energy and length respectively.)
- From the second term $[E] = [K][L]^3$ =$[M_s^2][L]^3$.

Comparing, we have $[A][L] = [K][L]^3 \rightarrow [A]/[K] = [L]^2$. We have that

$$\ell_{ex} = \sqrt{\frac{2A}{M_s^2}}.$$

Is a natural unit of length in this model.Define new space variables $\xi = x/\ell_{ex}, \ldots$ (similar for y, z) and obtain the energy expression

$$E = A\ell_{dw}\int \partial_\mu \mathbf{m} \cdot \partial_\mu \mathbf{m}\, d^3\xi + K\ell_{ex}^3\int (1 - m_3^2)\, d^3\xi. \tag{5.4.4}$$

Since $K\ell_{ex}^2 = A$, we obtain (set again $\xi \rightarrow x$ for simplicity)

$$E = 2A\ell_{dw}\left[\frac{1}{2}\int \partial_\mu \mathbf{m} \cdot \partial_\mu \mathbf{m}\, d^3x + \frac{1}{2}\int (1 - m_3^2)\, d^3x\right]. \tag{5.4.5}$$

The natural energy scale is $2A\ell_{dw}$.Let us summarize here the rationalized form of the energy terms discussed in this section. The total energy is the sum of the exchange + anisotropy energy

$$E = \frac{1}{2}\int \partial_\mu \mathbf{m} \cdot \partial_\mu \mathbf{m}\, d^3x + \frac{k^2}{2}\int (1 - m_3^2)\, d^3x. \tag{5.4.6}$$

where

$$k^2 = \frac{2K}{M_s^2}.$$

Let $\mathbf{m} = \mathbf{m}(x)$ correspond to a minimum of the energy.We apply a scaling in space $x \to \lambda x$ by a constant λ. Our magnetization configuration is now expanded.Then, for the magnetization $\mathbf{m}(\lambda x)$ we have the energy

$$E(\lambda) = \frac{1}{2}\int \partial_\mu \mathbf{m}(\lambda x)\cdot\partial_\mu \mathbf{m}(\lambda x)\, d^D x + \frac{k^2}{2}\int \left(1 - m_3^2(\lambda x)\right)\, d^D x \quad \mu = 1,2,3. \tag{5.4.7}$$

Since E is an extremum, it should also be an extremum with respect to scale transformations, when varying λ, at $\lambda = 1$

$$\frac{d}{d\lambda}E(\lambda)\big|_{\lambda=1} = \frac{d}{d\lambda}\left(\lambda^{2-D}E_{ex} + \lambda^{-D}E_{an}\right)_{\lambda=1} = 0. \tag{5.4.8}$$

This gives

$$\left[(2-D)\lambda^{1-D}E_{ex} - D\lambda^{-D-1}E_{an}\right]_{\lambda=1} = 0. \tag{5.4.9}$$

From the Derrick scaling argument, we finally obtain the virial relation

$$(2-D)E_{ex} = D\, E_{an}. \tag{5.4.10}$$

Since E_{ex}, E_{an} are positive definite, we conclude . For $D = 2$, only such energy minima exist for which $E_{an} = 0$, i.e., the only possible solutions are $\mathbf{m} = (0, 0, \pm 1)$.

Derrick's argument gives $E_{an} = 0$ and thus excludes all nontrivial (nonuniform) solutions. We can't find skyrmions in this model.

Chapter 6

Chiral skyrmionic Textures

6.1 Energy and equation of motion

We assume a ferromagnetic material as a two-dimensional system lying on the xy-plane. The micromagnetic structure is described via the magnetization vector $\mathbf{m} = \mathbf{m}(x, y)$ with a fixed magnitude normalized to unity, $\mathbf{m}^2 = 1$. We will assume a ferromagnet with exchange interaction, a Dzyaloshinskii-Moriya (DM) interaction, and an anisotropy of the easy-axis type perpendicular to the film, governed by the normalized energy

$$E = \frac{1}{2}\int \partial_\mu \mathbf{m} \cdot \partial_\mu \mathbf{m}\, dx + \frac{1}{2}\int (1 - m_3^2)\, dx + \lambda \int \mathcal{E}_{DM}\, dx. \tag{6.1.1}$$

A summation over repeated indices $\mu = 1, 2$ is assumed. The last term in the parenthesis in Eq. (6.1.1) models the DM interaction Prototypical cases are the bulk DM interaction form $\mathcal{E}_{DM} = \hat{e}_\mu \cdot (\partial_\mu \mathbf{m} \times \mathbf{m})$ and the interfacial DM interaction $\mathcal{E}_{DM} = \epsilon_{\mu\nu}\hat{e}_\mu \cdot (\partial_\nu \mathbf{m} \times \mathbf{m})$ form where $\epsilon_{\mu\nu}$ is the totally antisymmetric two-dimensional tensor. Here $\hat{e_1}, \hat{e_2}, \hat{e_3}$ are the unit vectors for the magnetization in the respective directions. Static magnetization fields are local minimizers of $\mathbf{E}$ satisfying the normalized Landau-Lifshitz equation

$$\mathbf{m} \times \mathbf{f} = 0, \tag{6.1.2}$$

where the effective field

$$\mathbf{f} = \partial_\mu \partial_\mu \mathbf{m} + m_3 \hat{e}_3 - 2\lambda \mathbf{f}_{DM},$$

where the last term is the DM field with $\mathbf{f}_{DM} = \hat{e}_\mu \cdot (\partial_\mu \mathbf{m} \times \mathbf{m})$ in case of bulk interaction or $\mathbf{f}_{DM} = \epsilon_{\mu\nu}\hat{e}_\mu \cdot (\partial_\nu \mathbf{m} \times \mathbf{m})$ in case of interfacial DM .

is minus the variational gradient of $E = E(\mathbf{m})$. We measure lengths in units of the domain wall width $\ell_w = \sqrt{A/K}$ where A is the exchange and K the anisotropy parameter. The equation contains a single parameter

$$\lambda = \frac{\ell_S}{\ell_w} = \frac{D}{2\sqrt{AK}}, \tag{6.1.3}$$

defined via an additional length scale of this model $\ell_S = D/(2K)$, where D is the DM parameter (a parameter which differs from λ only by a constant factor has been introduced).

6.2 Axially symmetric skyrmionic textures

Let us consider the angles (Θ, Φ) for the spherical parametrization of the magnetization vector, and the polar coordinates (ρ, ϕ) for the film plane. We assume an axially symmetric skyrmion with $\Phi = \phi + \phi_0$ and $\Theta = \Theta(\rho)$. For a bulk DM term the energy from Eq. (6.1.1) is minimized for $\phi_0 = \pi/2$ (Bloch skyrmion) and for interfacial DM interaction we choose $\phi_0 = 0$ (Neel skyrmion). A value $0 < \phi_0 < \pi/2$ should be chosen if the DM term is a combination of the bulk and interfacial terms . The skyrmion profile arises as a local minimizer of the energy

$$E = 2\pi \int_0^{+\infty} \left[\frac{1}{2}(\frac{d\Theta}{d\rho})^2 + \frac{1}{2}(1 + \frac{1}{\rho^2}\sin^2\Theta) + \lambda\left(\frac{d\Theta}{d\rho} + \frac{1}{2\rho}\sin 2\Theta\right)\right] \rho d\rho, \tag{6.2.1}$$

of

$$\mathbf{m}(\rho, \phi) = (\sin\Theta, \cos(\phi + \phi_0), \sin\Theta\sin(\phi + \phi_0), \cos\Theta),$$

whereby $\Theta = \Theta(\rho)$ satisfies the equation

$$\Theta'' + \frac{\Theta'}{\rho} - \frac{\sin(2\Theta)}{2\rho^2} + 2\lambda\frac{\sin^2\Theta}{\rho} - \frac{\sin(2\Theta)}{2} = 0, \tag{6.2.2}$$

with boundary conditions $\Theta(0) = \pi$ and $\lim_{\rho\to\infty}\Theta(\rho) = 0$. The same equation applies to all types of skyrmions, e.g., Bloch and Neel skyrmions for the respective DM terms.

6.2.1 Skyrmion

We can find the skyrmion numerically , within a model with exchange , anisotropy and DM interaction, a skyrmionic texture with Q = 1 , for the parameter value range $0 < \lambda < \frac{2}{\pi}$. We Choose lattice spacings $\delta x = \delta y = 0.1, 0.15, 0.2$, in most cases we use lattice space $\delta x = \delta y = 0.2$, then for values in between $0.15 \leq \lambda \leq 0.25$ we use lattice space $\delta x = \delta y = 0.15$ then as we get closer to $\lambda \approx 0$ we use $\delta x = \delta y = 0.1$ and also for the numerical meshes was fixed to 200×200 , 300×300 sites

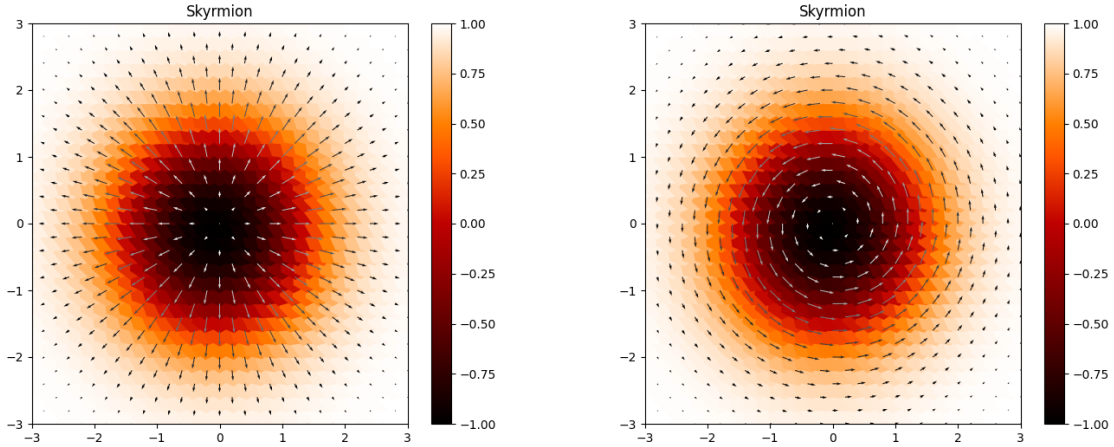

Figure 6.1: Two Skyrmions which find it numerically for lattice space $\delta x = \delta y = 0.2$ and lattice size 30×30 for value of DM parameter $\lambda = 0.5$, left configuration represent a condition with interfacial interaction and right represent a condition with bulk interaction . The static axially symmetric (Q = 1) skyrmion represented through the projection (m_1, m_2) of the magnetization vector on the plane for anisotropy $k = 1$.

Another interesting result is the dependence of the skyrmion radius on the parameter of the DM term. A formula for the skyrmion radius for small values of λ both E_{DM} and E_{an} are small while $E_{ex} > 4\pi$ (due to the topological energy bound). This leads to a skyrmion radius can be determined from the above results [11]

$$R = -\frac{\lambda}{\ln \lambda}. \tag{6.2.3}$$

Also a formula for the skyrmions of large radius [12]

$$R = \left(\frac{0.3057}{\frac{2}{\pi} - \lambda}\right)^{1/2}. \tag{6.2.4}$$

Numerical results show that the skyrmion radius increases with increasing λ and it diverges to infinity for $\lambda \to 2/\pi$, in agreement with theoretical results.

we compare the theoretical values with the numerical approximations and we plot the results in Fig. 6.2.4

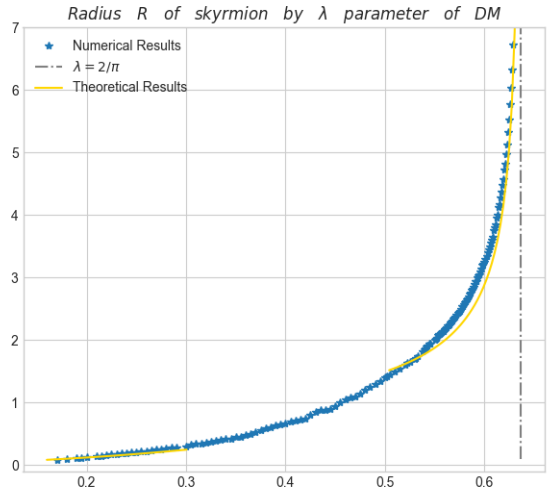

Figure 6.2: The figure represent the radius of skyrmion by the parameter λ of DM term.The blue line is the numerical approximations and gold line represent Eq. (6.2.3) and Eq. (6.2.4).

6.2.2 Skyrmionium

In magnetic systems, excitations can be found that are characterized by the orientation of the local magnetic moments of atomic cores. A magnetic skyrmionium is a ring-shaped topological spin texture and is closely related to the magnetic skyrmion. A magnetic skyrmionium is a topological quasi particle that is composed of a superposition of two magnetic skyrmions of opposite topological charge (A skyrmion with $Q = 1$ and an skyrmion with $Q = -1$) adding up to zero total topological charge $Q = 0$.

We are looking for axially-symmetric solutions of a model with exchange , anisotropy and DM term with skyrmion number $Q = 0$. An ansatz for a $Q = 0$ configuration is conveniently given in terms of the stereographic variable as

$$u = z - \frac{\alpha}{\bar{z}} \quad \text{or} \quad u = i(z - \frac{\alpha}{\bar{z}}), \tag{6.2.5}$$

where α is an arbitrary constant. The magnetization configuration produced by the form (6.2.5) is shown in Fig. 6.3 .

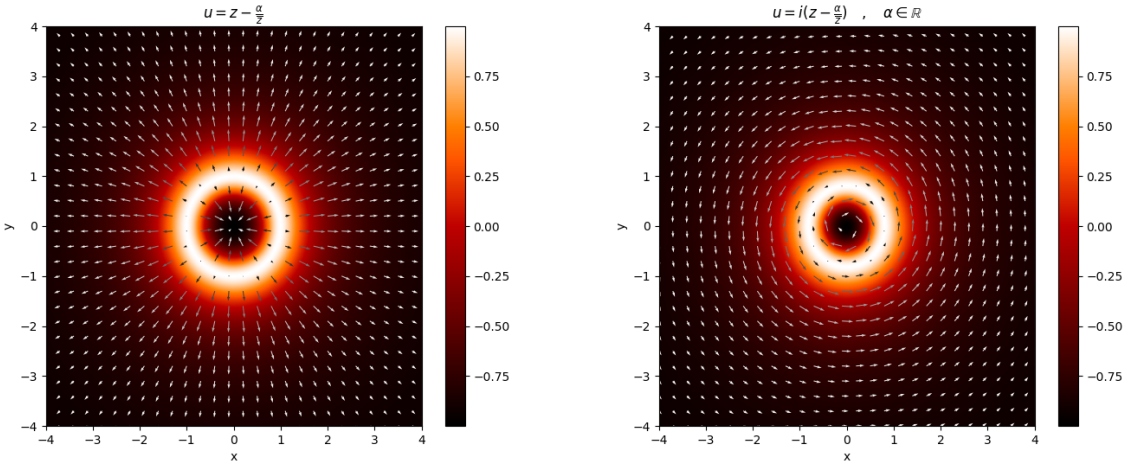

Figure 6.3: The static axially symmetric skyrmionium $(Q = 0)$ in interfacial condition (left) and bulk condition (right).

Skyrmionium isn't a static solution for Eq. (5.1.1) (like BP skyrmion) and form Eq. (6.2.5) don't satisfies the cauchy - Riemann equation , but we can find it numerically for the parameter value range $0.5 < \lambda < \frac{2}{\pi}$ and for initial condition with radius $\rho > 2.0$. We Choose latice spaces $\delta x = \delta y = 0.1, 0.15, 0.2$ and for the numerical meshes was fixed to 200×200 , 300×300 sites .

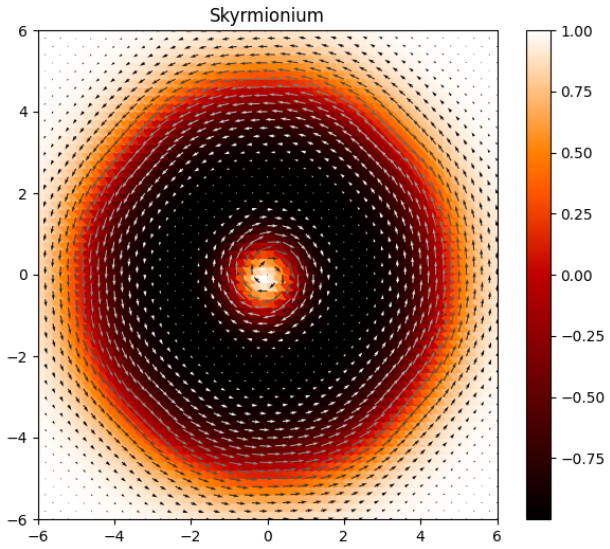

Figure 6.4: A skyrmionium which find it numerically for lattice space $\delta x = \delta y = 0.2$ and lattice size 30×30 for value of DM parameter $\lambda = 0.55$, configuration represent a condition with bulk DM interaction.The static axially symmetric skyrmionium (Q = 0) represented through the projection (m_1, m_2) of the magnetization vector on the plane for anisotropy $k = 1$.

Another interesting result is the dependence of the skyrmionium inner and outer radius on the parameter of the DM term.Numerical results show that the skyrmionium radius inner and outer increases with increasing λ and it diverges to infinity for $\lambda \to 2/\pi$ (See Fig. 6.5),also we noticed the inner radius reduced to zero when $\lambda \to 0.5$.

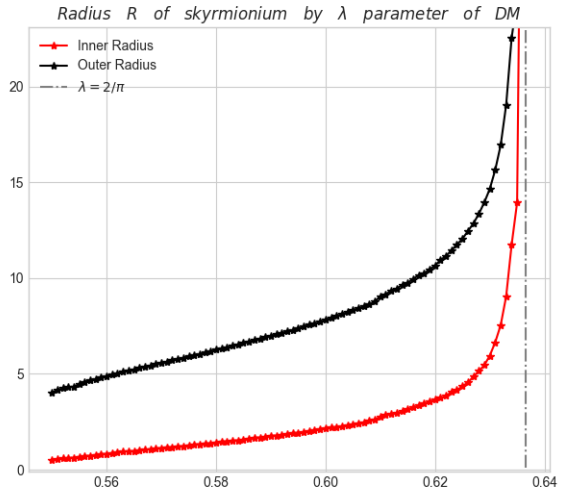

Figure 6.5: The figure represent the radius of skyrmionium inner (red) and outer (black) by the parameter λ of DM term .

6.3 Non-Axially Symmetric Skyrmionic textures

6.3.1 Droplet

We will study $Q = 0$ solitons that can be constructed as skyrmion-antiskyrmion pairs. Observations of topologically trivial objects in the form of skyrmionantiskyrmion pairs in a DM material are reported , $Q = 0$ textures are found numerically within a model with frustrated isotropic exchange and DM interaction and they are called "chiral skyrmions" due to the coexistence of skyrmion and antiskyrmion parts. We find numerically, within a model with DM interaction, a skyrmionic texture with $Q = 0$ that has the features of a skyrmion-antiskyrmion pair. This is an asymmetric configuration and its shape resembles that of a liquid droplet.

We are looking for solutions of a model with anisotropy and DM term with skyrmion number $Q = 0$. An ansatz for a $Q = 0$ configuration is conveniently given in terms of the stereographic variable as

$$u = \frac{\alpha}{x + i|y|} \quad \texttt{or} \quad u = \frac{\alpha}{|y| - ix}, \tag{6.3.1}$$

where α is an arbitrary constant. The magnetization configuration produced by the form Eq. (6.3.1) is shown in Fig. 6.6

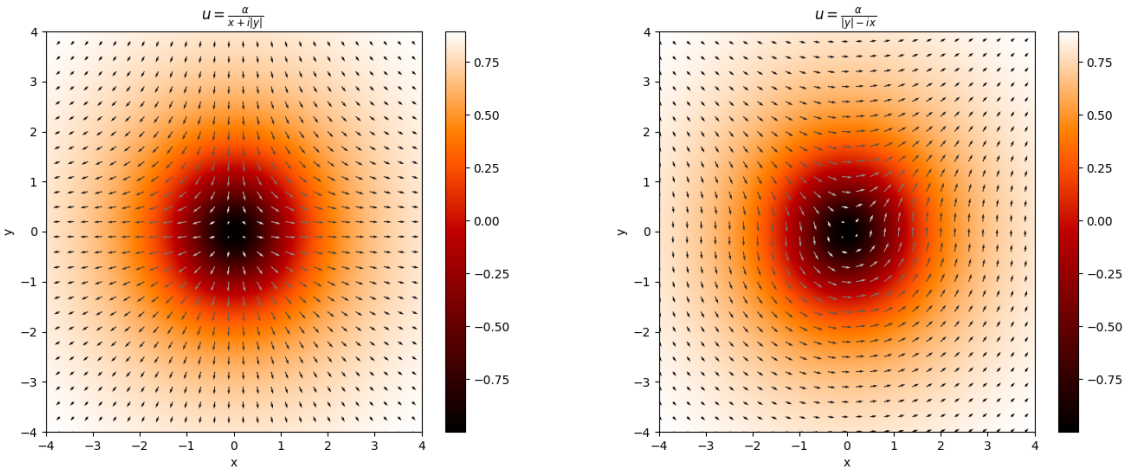

Figure 6.6: The static non-axially symmetric droplet $(Q = 0)$ in interfacial condition (left) and bulk condition (right).

The magnetization configuration Fig. 6.6 produced by the form Eq. (6.3.1) representing a skyrmion-antiskyrmion pair. The lower half of this configuration has the features of a skyrmion and the upper half has the features of an antiskyrmion.This is used as an initial condition in the energy relaxation algorithm for finding a static solution of the equation.

In most of the numerical simulations presented in the following figures, we use the set of parameter values shown in the following Table

Parameter	***Value***
M_s	$8.38 \times 10^5 A/m$
A	$1.1 \times 10^{-11} J/m$
K	$1.193(7.518) \times 10^6 J/m^3$
D	$3.5 \times 10^{-3} J/m^2$

Values for material parameters presented in the figures : M_s is the saturation magnetization, A the exchange parameter, K the easy-axis anisotropy parameter , and D the DM parameter. The above methodology converges to a static skyrmion-antiskyrmion configuration for a narrow range of values of the dimensionless parameters λ, κ . We find numerically the droplet for range of the values of the dimensionless parameters

$$0.6125 \leq \lambda < \frac{2}{\pi} \quad , \quad k = 1.0$$

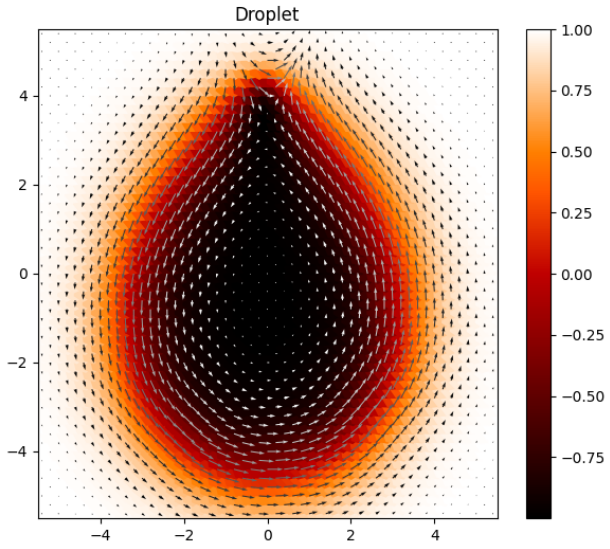

Figure 6.7: The figure represent a droplet which find it numerically with parameter of $\lambda = 0.62$ and latice space $\delta x = 0.2$ with lattice size 30×30 and bulk DM interaction.

Another interesting result is the dependence of the droplet energy on the parameter of the DM term.Numerical results show that the droplet energy discreases with increasing λ . We plot the results in Fig. 6.8 and remark we cannot find solutions of droplet for values of DM parameter smaller than $\lambda < 0.6$.

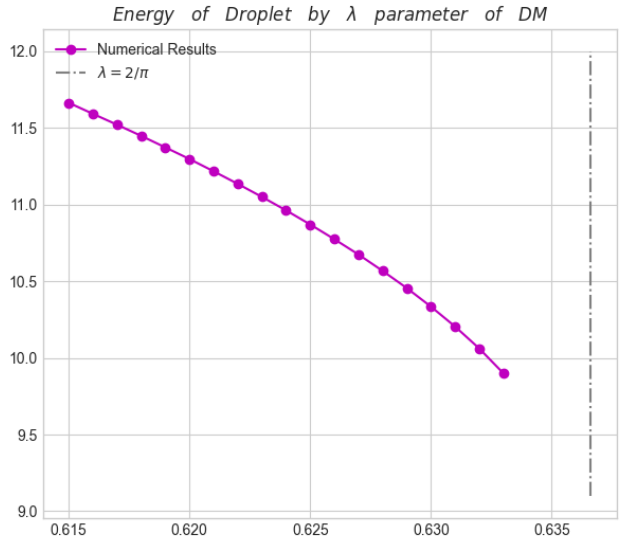

Figure 6.8: The energy of the droplet as a function of the DM parameter λ. Dots represent the numerical results and they are connected by a continuous line.

6.3.2 Bimeron

We will consider a model with exchange interaction, a Dzyaloshinskii-Moriya (DM) interaction, and an anisotropy of the easy-plane type perpendicular to the film , governed by the normalized energy

$$E = \frac{1}{2}\int \partial_\mu \mathbf{m}\cdot\partial_\mu \mathbf{m}\, d^2x + \frac{k^2}{2}\int m_3^2\, d^2x + \lambda \int \mathcal{E}_{DM}\, d^2x. \tag{6.3.2}$$

Static magnetization fields are local minimizers of $\mathbf{E}$ satisfying the normalized Landau-Lifshitz equation

$$\mathbf{m}\times\mathbf{f} = 0 \quad , \quad \mathbf{f} = \partial_\mu\partial_\mu \mathbf{m} - k^2 m_3 \hat{e}_3 - 2\lambda \mathbf{f}_{DM}, \tag{6.3.3}$$

We are looking for a non-axially symmetric solutions of this model with skyrmion number $Q_+ = 1/2$ and $Q_- = 1/2$ .An interesting object can be created if we assume that we have in a film a meron and an antimeron in proximity to each other.An ansatz for this skyrmion number configuration is conveniently given in terms of the stereographic variable

$$u = \frac{z-\alpha}{z+\alpha}, \tag{6.3.4}$$

where α is an arbitrary constant. The magnetization configuration produced by the form Eq. (6.3.4) is shown in following Figure

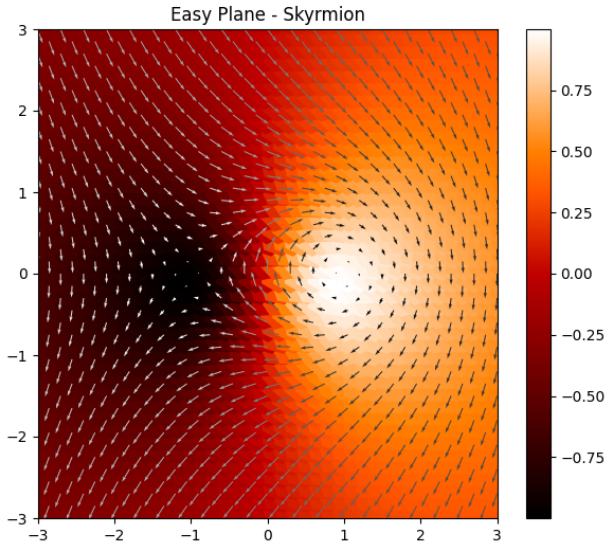

Figure 6.9: The static non-axially symmetric easy-plane skyrmion $Q_+ = 1/2$ and $Q_- = 1/2$ in bulk DM interaction.Vectors give the in-plane component of the magnetization vector (m_1, m_2).

The magnetization configuration Fig. 6.9 produced by the form Eq. (6.3.4) representing a meron-antimeron pair. The left part of configuration has the features of half-skyrmion with skyrmion number $Q_- = 1/2$ and the right part is the other half-skyrmion with skyrmion number $Q_+ = 1/2$ adding up to total topological charge $Q = 1$ .Its most important feature is that the magnetization is approaching a constant value at spatial infinity, e.g., $\mathbf{m}(\rho\to\infty)\to(1,0,0)$. This is because the

in-plane phases of the meron and the antimeron configurations cancel. Therefore we expect that, unlike a single meron or antimeron, a easy-plane skyrmion(Bimeron) has finite energy.

Easy-plane skyrmion We can find it numerically for easy-plane valye parameter $k = 1.0$ and the parameter of DMI value range $0.25 < \lambda < 2/\pi$. We Choose lattice spacing $\delta x = \delta y = 0.05, 0.075, 0.1, 0.15, 0.2, 0.5$ and for the numerical mesh was fixed to 200×200 , 300×300 sites.

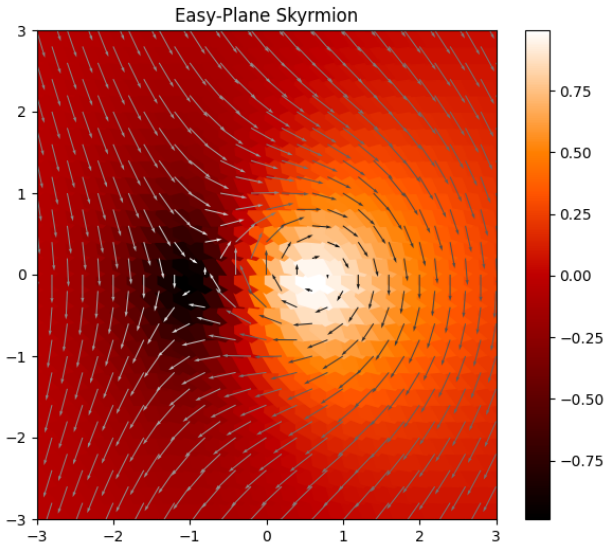

Figure 6.10: An easy-plane skyrmion (bimeron) found numerically as a static solution of the LL equation (6.3.3) including bulk DM interaction. We have used the DM parameter $\lambda = 0.35$ and easy-plane anisotropy $k = 1.0$. We have used lattice spacing $\delta x = \delta y = 0.2$ and a numerical mesh 300×300.

Another interesting result is the dependence of the bimeron energy on the parameter of the DM term.Numerical results show that the bimeron energy discreases with increasing λ ,we plot the results Fig. 6.11 and noticed the energy is almost equal with 4π when $\lambda \to 0.25$, in this case the energy of bimeron is $E \sim E_{ex}$ and using the Eq. (5.3.4) we conclude that we cannot find solutions of bimeron for values of DM parameter smaller than $\lambda < 0.25$.

One more observation is the following , bimeron hase transitions occur at the two critical values of the parameter

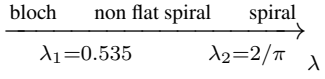

In this case when the paramater of DMI goes to first critical parameter λ_1 then the total energy of Bimeron goes to zero .

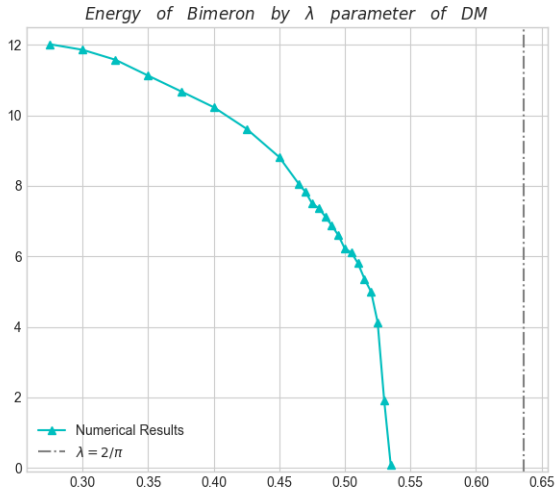

Figure 6.11: The energy of the bimeron as a function of the DM parameter λ. Dots represent the numerical results and they are connected by a continuous line.

Chapter 7

Applications in neuromorphic computing

7.1 Deep Neural Networks

The most proficiently used machine learning technique geared towards heavy data processing and pattern recognition is the DNN (Deep Neural Networks). This consists of simulated weighted graph networks where vertex values ascribed to each node (i.e. neuron) are sequentially updated via a normalized weighted sum of the node values feeding into it. These nodes can in turn be used to emulate any arbitrary vector function of some input subject to the edge weights being chosen accordingly. This process, known as training, effectively reduces to finding the minimizer of a complex cost function . DNN's have enjoyed wide acclaim for their ability at outperforming humans in tasks previously considered unattainable by machines.

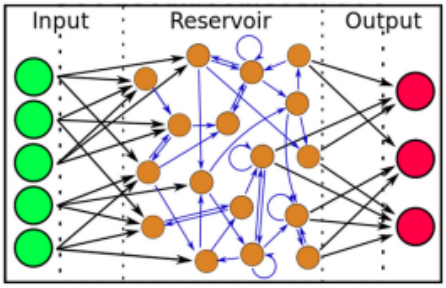

Figure 7.1: General schematic of reservoir computing for a recurrent neural network [Source[13]].

The most general class of DNNs, known as recurrent neural networks (RNNs) Fig. 7.1, considers coupled neurons whose graph representation consists of cycles forcing information to feedback (or echo) throughout the network and fade over time. This basic property allows RNNs to exhibit complex temporal dynamic behavior in response to the interplay of the instantaneous driving inputs and the RNN's implicit internal memory's echoing of past input information. Whereas the universal approximation theorem for feed-forward DNNs guarantees the faithful representation of any functio , the RNN's capacity to harness temporal correlations through their echo-state memories allows them to emulate universal Turing machines. This has far-reaching consequences as RNNs can be considered universal approximators of dynamical systems as a whole.

7.2 Reservoir Computing

however noticed that Hebbian training of RNNs mostly modifies just the output weights linking the bulk of the network to the read-out layer. These were the first to explicitly suggest the principle of employing a - mostly - randomly weighted RNN. The claim is that a sufficiently large RNN can be initialized with static random weights. Its training is then solely performed on a smaller set of weights associated with feed-forward connections between the bulk of the network and the output layer . Since such output weights consist of only a single layer connecting to the static RNN bulk (known as the reservoir), the training reduces to a linear regression performed on the reservoir state to satisfy a small training set of data. The advantage of this method, known as Reservoir Computing (RC), is not earned for free as the reservoir network has to typically be topologically more complex than an equivalent RNN fully trained to perform an identical task.

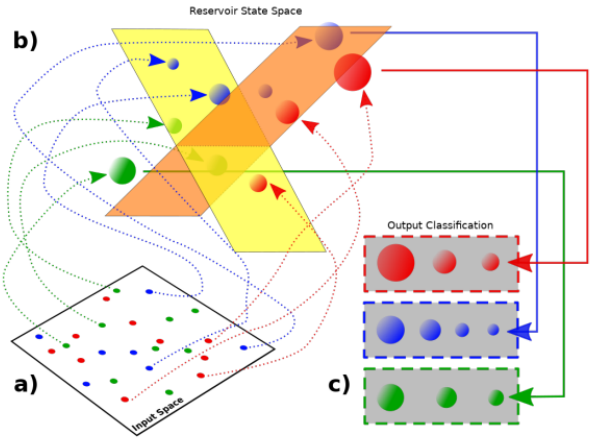

Figure 7.2: Schematic of the reservoir computing operational principle. (a) Unstructured data from an input space is (b) non-linearly projected by the reservoir's transient dynamics onto its higher dimensional state space. Due to the similar evolution of the reservoir when driven similarly correlated input data samples (represented by similar colors), (c) a single linear regression step can be used to define hyper-planes in the reservoir's state space such that different input data categories become separated. The task of the reservoir is to project different spatial-temporal events onto a sparsely populated high dimensional space where they become easier to recognize and categorize[Source[13].]

Generally speaking, a performant reservoir has the following properties:

- The dimension of the reservoir's phase space must be much larger than the size of the input category set.
- To guarantee reproducibility of its dynamical responses to identical inputs, the reservoir has to relax or be resettable to the same initial state once all inputs are removed.
- To ensure that memory of features fully affects the reservoir's evolution, any temporal feature correlations present in the input data must be of the same order as the natural transient dynamical timescale of the reservoir.

- The dynamics of the reservoir must be nonlinear but not ergodic to the point of strongly mixing trajectories throughout reservoir evolution.

- To properly identify all desired feature categories, a sufficiently large enough subspace of the reservoir state should be measurable.

The last requirement is particularly important in light of the dynamical systems interpretation used to justify reservoir computing. The feasibility of exploiting a physical system as a reservoir intimately depends on the technical ability to reliably inject input data and sample a sufficiently high dimensional subspace of the reservoir's state. To capture the reservoir's separation of N phase tubes corresponding to the number of input data categories, the output layer should be capable of generating a sufficient number hyper-planes to distinguish each phase tube pair

7.3 Magnetic systems as Reservoirs

There is no dearth of physical systems in nature which satisfy the general properties just discussed. Assessing, however, which systems may be industrially viable is an entirely different challenge. This work argues for the employment of magnetic textures due to their nanometer sizes, intricate dynamical properties and, most importantly, lowpower and CMOS-compatible all-electrical operability. In particular, we propose using random topological magnetic textures – skyrmion fabrics – to generate complex, high-dimensional representations of input voltage signals (Fig. 7.3).

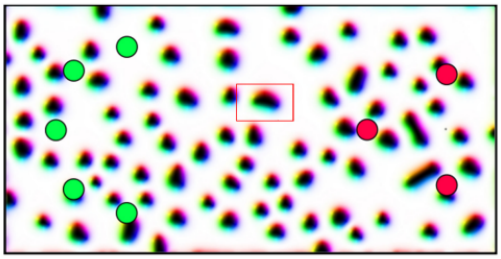

Figure 7.3: Example of a skyrmion fabric reservoir with locations of input (output) contacts identified by green (red) dots. The in-plane orientation of the magnetization is color coded[Source[13]].

Magnetic skyrmions are compact and metastable magnetic structures predicted over two decades ago and very actively studied experimentally both in lattice and isolated form Fig. 7.4 . The particlelike properties of skyrmions have been extensively summarized in several reviews . Their mobility under ultra-low current driving and room-temperature stability have garnered them a central position as information carriers in many device-relevant materials and applications

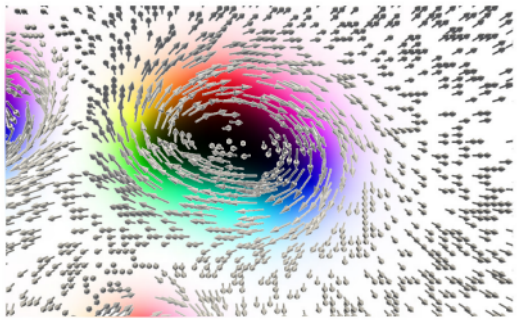

Figure 7.4: The figure represent shown in detail with arrows for a sample Bloch skyrmion identified by the red frame in Fig. 7.3 . The spatially extended nature of such a magnetic system allows for tunability in the number of electrical contacts. This allows to control the dimensionality of the reservoir snapshot[Source[13]].

Device oriented research has however mostly ignored intermediate skyrmion phases – known as "skyrmion fabrics" – which interpolate between single skyrmions, skyrmion crystals and magnetic domain walls . We claim that the random phase structure, complexity, nonlinear response, and memory characteristics present in skyrmion fabrics justify their use as a reservoir for RC. Gigahertz voltage patterns exciting the texture via nanocontacts can implement the injection of input information while the coupling of electron transport and magnetoresistivity can be used to sample the magnetic state of the system.

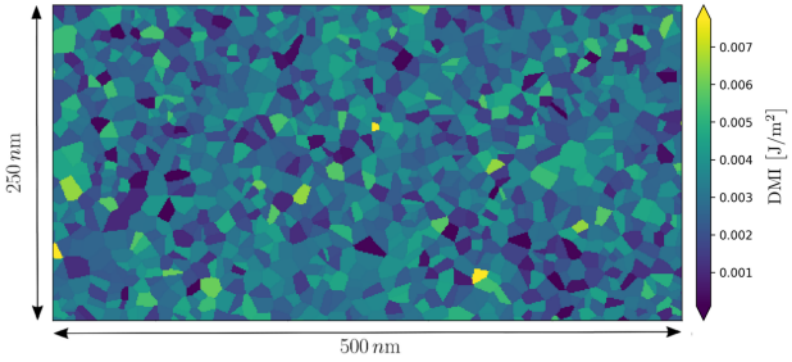

Figure 7.5: Randomly generated DMI-grain inhomogeneities employed to pin skyrmions. Figure shown corresponds to a 250×500 nm geometry consisting of 10 nm grains exhibiting a 40% DMI variance around a $0.003\,\mathrm{J/m^2}$ mean value[Source[13]].

7.4 Skyrmion fabric reservoir model

For the sake of simplicity, we consider a random magnetic skyrmion phase in a spatially extended rectangular geometry with only two voltage contacts. To model a realistic setup, our sample is subject to Dzyaloshinskii-Moriya interaction(DMI) via grain inhomogeneities and a static applied magnetic field (Fig. 7.5) A random magnetic texture is generated by imposing an initial skyrmion

lattice structure and allowing it to freely relax (Fig. 7.6) .The introduced magnetic inhomogeneities have been extensively studied in the literature as a source of skyrmion pinning to explain the discrete onset of the creep threshold in skyrmion mobility both theoretically and in experiments. Initialization is considered complete when the magnetic texture has relaxed to a stable state and does not change significantly when subject to thermal noise and a constant applied voltage across the electrical contacts. The voltage magnitude is chosen such that the resulting magnetization dynamics lie just below the skyrmion creep threshold where their deformations are maximal.

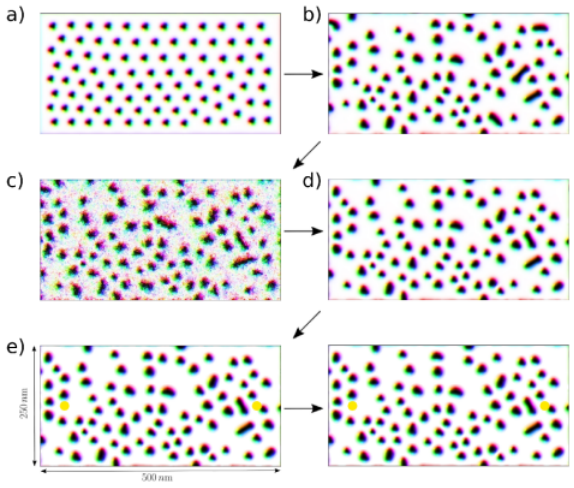

Figure 7.6: Initialization of magnetic texture and thermal stability test. (a) An artificial skyrmion lattice is generated. (b) The lattice is relaxed under the effect of an applied external magnetic field and DMI grain inhomogeneities. (c) Thermal noise is added and allowed to act for 20 ns before being switched off. (d) The magnetic texture is relaxed again in the absence of thermal noise. (e) A 20 ns constant voltage pulse is applied to verify that skyrmions are not displaced by current-mediated transport effects. The relaxed magnetic configurations in (b) and (d) are compared to verify that the majority of skyrmions appearing in the bulk of the geometry are not significantly affected by thermal effects[Source[13]].

As aforementioned, the magnetic texture is excited via time-varying voltage patterns injected through the nanocontacts . Due to the sub-creep setup described, such patterns will excite time dependent deformations of the magnetic skyrmion texture due to a variety of magnetoresistive effects. Since the natural electron relaxation timescale is orders of magnitude smaller than the ferromagnetic resonance (FMR) timescale ($\sim 10^{-14}s$ vs. $\sim 10^{-9}s$), these effects will guarantee that a given state of the magnetic texture will result in a unique corresponding current distribution throughout the geometry. To simplify the modeling of such electron-transport mediated effects and isolate their qualitative nature, we will focus solely on the anisotropic magnetoresistance (AMR) effect.

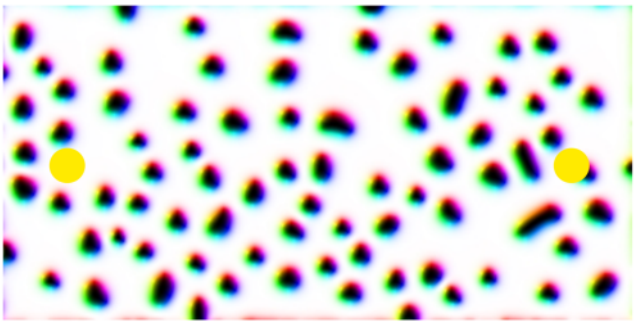

Figure 7.7: Sample skyrmion texture used for simulations. The locations of the electrical nanocontacts are identified by the yellow disks (size has been enhanced for visibility)[Source[13]].

Current densities are calculated self-consistently through $\mathbf{j}[U, \mathbf{m}] = -\sigma[\mathbf{m}] \cdot \mathbf{E}[U]$ at each time step of the magnetization's Landau-Lifshitz-Gilbert (LLG) dynamics. The electric field through the texture, induced by the applied voltage, is calculated by solving the Poisson equation $\mathbf{E} = -\nabla\mathbf{\Phi}$ with boundary conditions $\mathbf{\Phi}|_{c1} = -\mathbf{\Phi}|_{c2} = U$ at the two contacts, and the conductivity tensor

$$\sigma[\mathbf{m}] = \frac{1}{\rho_\perp}\mathbf{1} + (\frac{1}{\rho_{||}} - \frac{1}{\rho_\perp})\mathbf{m} \otimes \mathbf{m}. \tag{7.4.1}$$

Is computed at each point throughout the geometry. We denote by $\rho_\perp(\rho_{||})$ the current resistivities for flows perpendicular (parallel) to the magnetization direction. For definiteness the results in the next section consider the typical case where $\rho_\perp > \rho_{||}$. An example of an excited skyrmion fabric is shown in Fig. 7.7 right above a density plot of the instantaneous current distribution traversing it (Fig. 7.8).

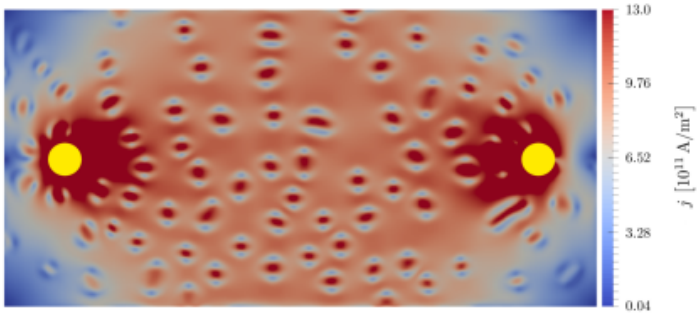

Figure 7.8: Sample relaxed current distribution through the texture shown in Fig. 7.7 when a 110 mV potential difference is applied across the nanocontacts[Source[13]].

Chapter 8

Conclusions

In conclusion, we studied static solutions in 2-dimensions of micromagnetic phenomena in models on the sphere (heisenberg models). We considered and studied a model with exchange,anisotropy (easy-axis and easy-plane) and Dzyaloshinskii-Moriya (DM) interaction .

Especially the Dzyaloshinskii-Moriya (DM) term gived to us the possibility to found and studied Skyrmionic textures solutions for realist models in micromagnetics .We noticed this solutions depends by the range of value for this parameter (we refer to this to λ-parameter for this thesis) .

We started our computations for axially and non-axially symmetric configurations and we compared our numerical result with BP-Skyrmions which is statics solutions for only a model with exchange interaction and it is very important result which found it at early 60's . Furthermore we manage to find solutions for chiral skyrmion which were found from scientists at last years with topological skyrmion number $Q = 0, \pm 1$ and energy boundaries for every single configuration .

More specific we found axially symmetric skyrmionic textures which called skyrmion ($Q = \pm 1$) and skyrmionium ($Q = 0$) and we calculated the exact range value of λ-Parameter which could find it .In addition we made the same work for non-axially symmetric skyrmionic textures which called Droplet ($Q = 0$) and Bimeron ($Q = 1$), especially Bimeron is interesting solution because is a skyrmionic textures solution with easy-plane anisotropy and they do not exist exact result about this configuaration from bibliography .

Last but not least we studied and introduced some ideas about neuromorphic computing and how to trained and built neural networks for magnetic systems .

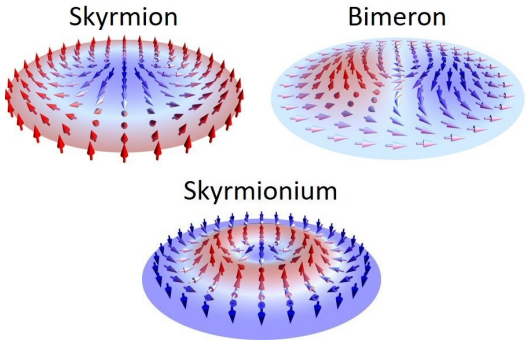

Figure 8.1: The figure represent a skyrmion , a bimeron and skyrmionium [14].

Acknowledgement

I want to give special thanks Mr.Stavros komineas for advice and guidance from the beginning of this thesis ,as well all members of the ThunderSky project in FORTH especially George,Nikos and Panos for duscusions about scientific and more subects . Furthermore i want to thanks all my friends Dimitra,Agapi,Katianna,Marina,Konstantina,Petros,George,Tasos,Chris and my parents Spyridoula and George for supporting all of this years and i hope managed to made you proud .

Appendix A

Calculus of Variations

A.1 Fuctionals

Variable quantities called functionals play an important role in many problems arising in analysis, mechanics, geometry, etc. By a functional, we mean a correspondence which assigns a definite (real) number to each function (or curve) belonging to some class. Thus, one might say that a functional is a kind of function, where the independent variable is itself a function (or curve). The following are examples of functionals:

- 1. Consider the set of all rectifiable plane curves. A definite number is associated with each such curve, namely, its length. Thus, the length of a curve is a functional defined on the set of rectifiable curves.
- 2. Suppose that each rectifiable plane curve is regarded as being made out of some homogeneous material. Then if we associate with each such curve the ordinate of its center of mass, we again obtain a functional.
- 3. Consider all possible paths joining two given points A and B in the plane. Suppose that a particle can move along any of these paths, and let the particle have a definite velocity $v(x, y)$ at the point (x, y) . Then we obtain a functional by associating with each path the time the particle takes to traverse the path.
- 4. Let $y(x)$ be an arbitrary continuously differentiable function, defined on the interval $[a, b]^2$ Then the formula

$$\mathcal{J}[y] = \int_a^b y'^2 \, dx,$$

  defines a functional on the set of all such functions $y(x)$.
- 5. As a more general example, let $F(x, y, z)$ be a continuous function of three variables. Then the expression

$$\mathcal{J}[y] = \int_a^b F[x, y(x), y'(x)] \, dx,$$

where $y(x)$ ranges over the set of all continuously differentiable functions defined on the interval $[a, b]$, defines a functional. By choosing different functions $F(x, y, z)$, we obtain different functionals.

Particular instances of problems involving the concept of a functional were considered more than three hundred years ago, and in fact, the first important results in this area are due to Euler (1707-1783). Nevertheless, up to now, the " calculus of functionals" still does not have methods of a generality comparable to the methods of classical analysis (Le. , the ordinary " calculus of functions"). The most developed branch of the " calculus of functionals" is concerned with finding the maxima and minima of functionals, and is called the " calculus of variations." Actually, it would be more appropriate to call this subject the " calculus of variations in the narrow sense," since the significance of the concept of the variation of a functional is by no means confined to its applications to the problem of determining the extrema of functionals.

A.2 Function Space

In the study of functions of n variables, it is convenient to use geometric language, by regarding a set of n numbers $(y_1, \ldots, y_n)$ as a point in an n-dimensional space. In just the same way, geometric language is useful when studying functionals. Thus, we shall regard each function y(x) belonging to some class as a point in some space, and spaces whose elements are functions will be called function spaces. In the study of functions of a finite number n of independent variables, it is sufficient to consider a single space, i.e., n-dimensional Euclidean space $\mathbf{E}$.

However, in the case of function spaces, there is no such " universal" space. In fact, the nature of the problem under consideration determines the choice of the function space. For example, if we are dealing with a functional of the form

$$\int_a^b F(x, y, y')\, dx,$$

it is natural to regard the functional as defined on the set of all functions with a continuous first derivative, while in the case of a functional of the form

$$\int_a^b F(x, y, y', y'')\, dx,$$

the appropriate function space is the set of all functions with two continuous derivatives. Therefore, in studying functionals of various types, it is reasonable to use various function spaces.

The concept of continuity plays an important role for functionals, just as it does for the ordinary functions considered in classical analysis. In order to formulate this concept for functionals, we must somehow introduce a concept of " closeness" for elements in a function space. This is most conveniently done by introducing the concept of the norm of a function, analogous to the concept of the distance between a point in Euclidean space and the origin of coordinates. Although in what follows we shall always be concerned with function spaces, it will be most convenient to introduce the concept of a norm in a more general and abstract form, by introducing the concept of a normed linear space.

By a linear space, we mean a set $\mathbb{R}$ of elements $x, y, z, \ldots$ of any kind, for which the operations of addition and multiplication by (real) numbers $\alpha, \beta, \ldots$ are defined and obey the following axioms:

- 1. $x + y = y + x$
- 2. $x + (y + z) = (x + y) + z$
- 3. $x + 0 = x$
- 4. $x + (-x) = 0$
- 5. $1 \cdot x = x$
- 6. $\alpha(\beta x) = (\alpha\beta)x$
- 7. $(\alpha + \beta)x = \alpha x + \beta x$
- 8. $\alpha(x + y) = \alpha x + \beta y$

A linear space $\mathbb{R}$ is said to be normed, if each element $x \in \mathbb{R}$ is assigned a nonnegative number $\|x\|$, called the norm of x , such that

- 1. $||x|| = 0$ if and only if $x = 0$
- 2. $||ax|| = |a|\,||x||$
- 3. $||x + y|| \leq ||x|| + ||y||$

In a normed linear space, we can talk about distances between elements, by defining the distance between x and y to be the quantity $\|x - y\|$. The elements of a normed linear space can be objects of any kind, e.g., numbers, vectors (directed line segments), matrices, functions, etc.

A.3 The Variation of a Functional

We now introduce the concept of the variation (or differential) of a functional. Let $J[y]$ be a functional defined on some normed linear space, and let

$$d\mathcal{J}[h] = \mathcal{J}[y + h] - \mathcal{J}[y],$$

be its increment, corresponding to the increment h = hex) of the " independent variable " $y = y(x)$. If y is fixed, $\Delta\mathcal{J}[h]$ is a functional of h , in general a nonlinear functional. Suppose that

$$d\mathcal{J}[h] = \phi[h] + \epsilon||h||,$$

where $\phi[h]$ is a linear functional and $\epsilon \to 0$ as $\|h\| \to 0$. Then the functional $\mathcal{J}[y]$ is said to be differentiable, and the principal linear part of the increment $\Delta\mathcal{J}[h]$, i.e., the linear functional $\phi[h]$ which differs from $\Delta\mathcal{J}[h]$ by an infinitesimal of order higher than 1 relative to $||h||$, is called the variation (or differential) of $\mathcal{J}[y]$ and is denoted by $\Delta\mathcal{J}[h]$.

A.4 The Simplest Variational Problem. Euler's Equation

We begin our study of concrete variational problems by considering what might be called the "simplest " variational problem, which can be formulated as follows: Let $F(x, y, z)$ be a function with continuous first and second (partial) derivatives with respect to all its arguments. Then, among all functions $y(x)$ which are continuously differentiable for $a \leq x \leq b$ and satisfy the boundary conditions

$$y(a) = A \quad , \quad y(b) = B,$$

find the function for which the functional

$$\mathcal{J}[y] = \int_a^b F(x, y, y')\, dx,$$

has a weak extremum. In other words, the simplest variational problem consists of finding a weak extremum of a functional of the form , where the class of admissible curves consists of all smooth curves joining two points. To apply the necessary condition for an extremum to the problem just formulated, we have to be able to calculate the variation of a functional of the type . We now derive the appropriate formula for this variation

Suppose we give $y(x)$ an increment $h(x)$, where, in order for the function

$$y(x) + h(x),$$

to continue to satisfy the boundary conditions, we must have

$$h(a) = h(b) = 0,$$

Then, since the corresponding increment of the functional equals

$$\Delta\mathcal{J} = \mathcal{J}[y + h] - \mathcal{J}[y] = \int_a^b [F(x, y + h, y' + h') - F(x, y, y')]\, dx,$$

it follows by using Taylor's theorem that

$$\Delta\mathcal{J} = \int_a^b [F_y(x, y, y')h - F_{y'}(x, y, y')h'] \quad dx + \ldots$$

where the subscripts denote partial derivatives with respect to the corresponding arguments, and the dots denote terms of order higher than 1 relative to h and h' . The integral in the right-hand side of represents the principal linear part of the increment $\Delta\mathcal{J}$, and hence the variation of $\mathcal{J}[y]$ is

$$\delta\mathcal{J} = \int_a^b [F_y(x, y, y')h - F_{y'}(x, y, y')h']\, dx,$$

a necessary condition for $\mathcal{J}[y]$ to have an extremum for $y = y(x)$ is that

$$\delta\mathcal{J} = \int_a^b [F_y(x, y, y')h - F_{y'}(x, y, y')h']\, dx = 0,$$

for all admissible h . But implies that

$$F_y - \frac{d}{dx}F_{y'} = 0,$$

a result known as Euler's equation.

Theorem 1. Let $\mathcal{J}[y]$ be a functional of the form

$$\mathcal{J}[h] = \int_a^b F(x, y, y')\, dx,$$

defined on the set of functions $y(x)$ which have continuous first derivatives in $[a, b]$ and satisfy the boundary conditions $y(a) = A$, $y(b) = B$. Then a necessary condition for $\mathcal{J}[y]$ to have an extremum for a given function $y(x)$ is that $y(x)$ satisfy Euler's equation.

The integral curves of Euler's equation are called extremals. Since Euler's equation is a second-order differential equation, its solution will in general depend on two arbitrary constants, which are determined from the boundary conditions $y(a) = A$, $y(b) = B$. The problem usually considered in the theory of differential equations is that of finding a solution which is defined in the neighborhood of some point and satisfies given initial conditions (Cauchy's problem). However, in solving Euler's equation, we are looking for a solution which is defined over all of some fixed region and satisfies given boundary conditions. Therefore, the question of whether or not a certain variational problem has a solution does not just reduce to the usual existence theorems for differential equations.

A.5 Hamilton Principle

Hamilton published two papers in 1834 and 1835, announcing a fundamental new dynamical principle that underlies both Lagrangian and Hamiltonian mechanics. Hamilton was seeking a theory of optics when he developed Hamilton's Action Principle, plus the field of Hamiltonian mechanics, both of which play a crucial role in classical mechanics and modern physics. Hamilton's Action Principle states "dynamical systems follow paths that minimize the time integral of the Lagrangian". That is, the action functional $\mathcal{I}$

$$\mathcal{I} = \int_{t_1}^{t_2} L(x, \dot{x}, t)\, dt,$$

has a minimum value for the correct path of motion. Hamilton's Action Principle can be written in terms of a virtual infinitessimal displacement δ, as

$$\delta\mathcal{I} = \delta \int_{t_1}^{t_2} L(x, \dot{x}, t)\, dt = 0.$$

Variational calculus therefore implies that a system of s independent generalized coordinates must satisfy the basic Euler-Lagrange equations

$$\frac{\partial L}{\partial x} - \frac{d}{dt}\left(\frac{\partial L}{\partial \dot{x}}\right) = 0.$$

Appendix B

Magnetic Vortices

B.1 Ordinary vortices in fluids

We know from common experience that vortices are pervasive in nature and they play a significant role in various physical systems. The most well known examples appear in fluids where fluid vortices play a central role in the description and understanding of the motion of fluids, including complicate dynamical phenomena such as turbulent flow.

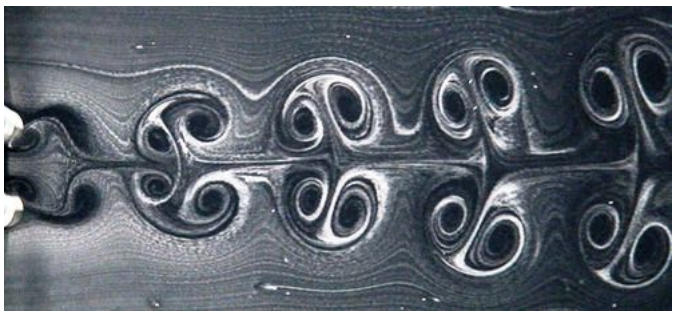

Figure B.1: A series of vortices in a fluid. The fluid may rotate clockwise or anticlockwise around the vortex center. The vortices may be bigger or smaller

The description of the motion of fluids is based on non-linear partial differential equations. It is though possible to reduce these equations to much simpler forms if we want to describe, within some approximation, the motion of a vortex which is located away from other vortices. In that case we assume that the area of the vortex is small compared to the distance to other vortices. We then approximate the vortex position by a single point and we call this the point vortex approximation. A significant quantity for the description of vortices is the local vorticity (γ) defined at every point of the fluid and it is the rotation of its velocity ($\nabla \times \mathbf{u}$). The total vorticity is the integral of the vorticity over the area of the fluid.

$$\Gamma = \int \gamma \, dxdy, \tag{B.1.1}$$

and it is considered as the strength of the vortex. It is interesting that it can be shown that the

following are conserved quantities in vortex motion:

$$I_x = \int x\gamma \, dxdy \quad I_y = \int y\gamma \, dxdy, \tag{B.1.2}$$

It is evident that these quantities can be considered to give the position of a vortex (if we normalize by Γ). For example, in the case of point vortices, the above integrals just give the vortex position multiplied by its strength (total vorticity)

B.2 Quantized vortices in superfluids

Some fluids exhibit unusual properties when they are in very low temperatures. Probably their most impressive property is that they can flow without dissipation, that is without their motion be decelerated. Such fluids are called superfluids. Superfluidity was first observed in liquid helium in temperatures $T < 2.7$ Kelvin. More recently (1995) superfluid gases in the form of vapours of alkali metals (Li, Na, K, Rb, Cs) have been obtained and experimentally studied. Vapours of alkali metals are typically trapped by magnetic and optical (laser) fields and they are subsequently cooled by a series of techniques to temperatures $T \approx 10 - 100$ nanoKelvin. Such atomic gases are extremely dilute and a typical trap may contain $105 - 106$ atoms confined in spatial dimensions of the order of 10 μm.

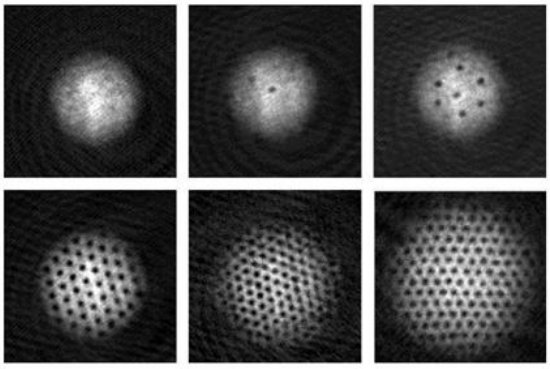

Figure B.2: Vortices in a BEC. The dark spots are the cores of the vortices .

An additional property of superfluids is that superfluid vortices have strength which may only be an integer multiple of a basic quantity and we call these quantized vortices. This property of vortices is related to their property of frictionless flow. Superfluids are studied using quantum mechanics. In some cases one can approximate superfluid dynamics by non-linear partial differential equations (Gross-Pitaevskii model). These equations differ significantly from those for ordinary fluids. One important point is that the vorticity in superfluid is related to topological features of the field which describes the superfluid (i.e., the complex wavefunction which describes the superfluid). One can define a vorticity, where the total vorticity Eq. (B.1.1) takes only discrete values and it can be interpreted as a topological number. Conserved quantities formally identical to Eq. (B.1.2) exist also in the present case. Furthermore, the point vortex approximation can be employed in this system, too, and obtain simple differential equations for the vortex motion.

B.3 Magnetic vortices

Although we tend to link vortices with fluid motion, the case is that vortices appear in many systems which may not present physical fluid motion, as mathematical structures of vector fields. An interesting example are magnetic materials where we have magnetic vortices.

The microscopic structure in a magnetic material is described by the magnetization vector $\mathbf{m}(x, y)$. As interesting question is the following: what are the structures formed by the magnetization vector (which is actually a vector field) and what is their dynamics? The answers to such questions are important, for example, when we would like to store and retrieve information from a magnetic disc, since the information is stored as particular magnetization structures. We need to know the dynamics of such structures if we want to be able to change them in a controlled way.

Although there is no physical fluid flow in magnetic materials, we can define a quantity n which has properties corresponding to the fluid vorticity (γ). The magnetic vorticity n is related to topological features of the magnetization and the total vorticity

$$\mathcal{N} = \int n \, dxdy, \tag{B.3.1}$$

is an integer multiple of a basic quantity. We finally mention that we have conserved quantities of the motion

$$I_x = \int xn \, dxdy \quad I_y = \int yn \, dxdy, \tag{B.3.2}$$

which are formally similar to the conserved quantities for fluids in Eq. (B.1.2). It can also be shown that, if we make a point vortex approximation, the dynamics of magnetic vortices is modeled by equation similar to those for point fluid vortices.

B.4 Axially symmetric vortex

For any nontrivial (nonuniform) magnetic configuration we would require that $\mathbf{m}(|r| \to \infty) \to \mathbf{m}_0$, that is, the magnetization tends to a ground state configuration at spatial infinity. This is because, otherwise the magnetic configuration would have infinite energy and it would be unstable. On the other hand, any nontrivial configuration for which the magnetization goes to a certain uniform magnetization at spatial infinity is excluded by Derrick's argument.

In order to construct a nontrivial magnetic configuration we will exploit the infinite degeneracy of the ground state in-plane configurations. We impose the boundary condition at spatial infinity

$$m_1 + im_2 = e^{i(\phi+\phi_0)}, \quad m_3 = 0, \qquad \text{for} \quad \rho \to \infty. \tag{B.4.1}$$

where (ρ, ϕ) are polar coordinates and ϕ_0 is a constant angle. The magnetisation points in different directions, at spatial infinity, if we look at different angles.

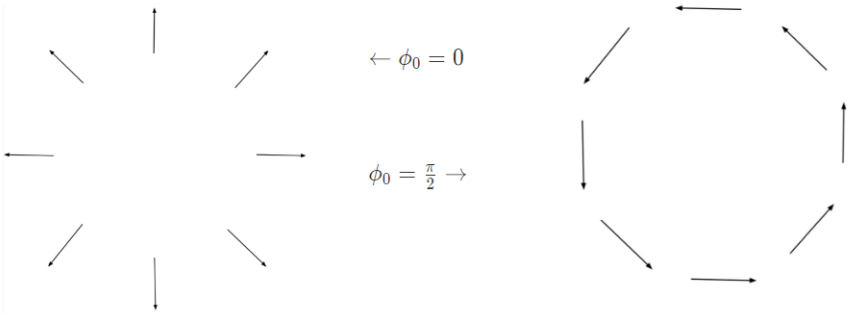

Figure B.3: The magnetisation vector rotates as we make a rotation (in real space) around the origin.

A configuration which is consistent with the boundary condition Eq. (B.4.1) is given by the following axially symmetric ansatz, using the angle variables

$$m_1 + im_2 = \sin\Theta(\rho)\, e^{i(\phi+\phi_0)}, \quad m_3 = \cos\Theta(\rho). \tag{B.4.2}$$

We have assumed that $\Theta = \Theta(\rho)$ (i.e., axial symmetry) while we implicitly set the angle variable $\Phi = \phi + \phi_0$. The energy is written as

$$E = \frac{1}{2}\int_0^\infty \left[(\Theta')^2 + \frac{\sin^2\Theta}{\rho^2} + k^2\cos^2\Theta\right](2\pi\rho d\rho). \tag{B.4.3}$$

B.5 Winding number

The most important feature of the vortex solution is that the magnetization has a different orientation in the xy-plane for different locations in space, even when we are away from the vortex center. More specifically, we can choose a circle with its center at the vortex core and we go around the circle registering the in-plane component of the magnetization (m_1, m_2) at each point. One should note that the in-plane magnetization vector can be characterized by the single angle Φ, that is, every vector orientation corresponds to a point on a circle. Therefore, as we go around a vortex rotating, say, anticlockwise on a circle in physical space, we measure an angle ϕ for the magnetization. In this way we can define a mapping from the physical space to the magnetization space, this being a mapping from a circle to a circle.

In the case of the vortex presented in the previous subsection a full rotation (anticlockwise) around the vortex center gives a corresponding full rotating (again anticlockwise) of the magnetization vector on the xy-plane, or $\Delta\Phi = 2\pi$. We assign to the vortex a winding number $\mathcal{N}$ which represents this particular vortex feature. We define $\mathcal{N} = \Delta\Phi/2\pi$, so the single full rotation of the magnetization vector is denoted by saying the $\mathcal{N} = 1$. The magnetization vector on the plane (m_1, m_2) for a vortex is plotted in Fig. B.4 for $\phi_0 = 0$, and in Fig. B.5 for a vortex with $\phi_0 = \pi/2$.

It is evident that as we go around a full circle in physical space, physical quantities must be the same when we return to the initial point, therefore for the difference of the angle Φ of the magnetization we have $\Delta\Phi = (2\pi)\mathcal{N}$ with $\mathcal{N} = 0, \pm1, \pm2, \ldots$ We assume the following more general vortex

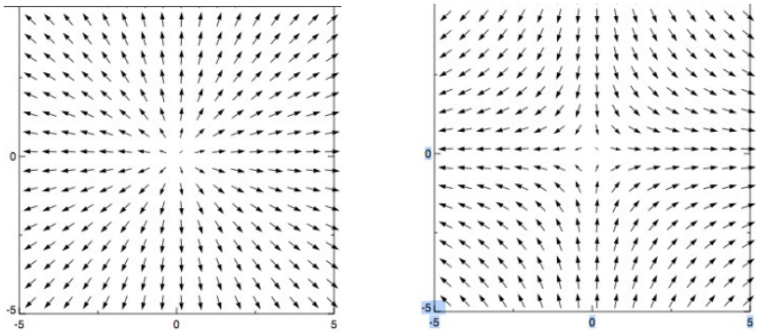

Figure B.4: A vortex configuration ($\mathcal{N} = 1$) with $\phi_0 = 0$. (Right) An antivortex configuration with ($\mathcal{N} = -1$) $\phi_0 = 0$. We plot the projection of the magnetization on the plane: (m_1, m_2). The magnetization in the center of the figure is supposed to point either "up" or "down', that is, $\mathbf{m} = (0, 0, \lambda)$ where $\lambda = \pm 1$ is the vortex polarity.

ansatz

$$m_1 + im_2 = \sin\Theta(\rho)\, e^{i\mathcal{N}(\phi+\phi_0)}, \quad m_3 = \cos\Theta(\rho). \tag{B.5.1}$$

The case $\mathcal{N} = 1$ corresponds to the vortex discussed above, while in the case $\mathcal{N} = -1$ we will call the configuration an antivortex (Fig. B.4). The equation satisfied by the angle θ for the antivortex is identical to that for the vortex and therefore the antivortex profile coincides with that of the vortex . As a consequence, the antivortex energy Eq. (B.4.3) (when we take into account exchange and anisotropy only) is identical to that of the vortex. The case $\mathcal{N} = \pm 2$ gives an object which may be called a double vortex or antivortex. We can apply the same methods as for the vortex in order to find the profile of a double vortex and its energy. However, it turns out that this is typically an unstable configuration which tends to split into two separate vortices. This is apparently due to the exchange energy which is approximately proportional to S^2 so that the energy of a double vortex is higher that that of two single vortices.

The winding number $\mathcal{N}$ is a topological invariant which can be defined as the degree of a mapping from the circle to the circle . It is for this reason that it may only take integer values. The winding number cannot change during the motion of the system because this would imply a discontinuous change of the magnetization configuration. Furthermore, $\mathcal{N}$ is a conserved quantity, that is, it remains constant under the dynamics prescribed by the model. It is not important to specify what the particular dynamics is, it suffices that this be continuous.

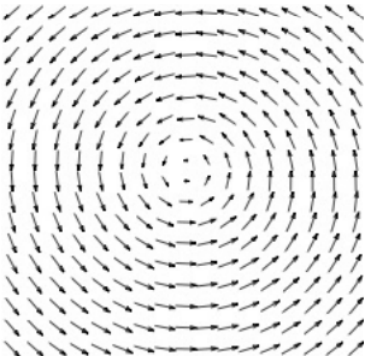

Figure B.5: A vortex configuration ($\mathcal{N} = 1$) with $\phi_0 = \pi/2$. We plot the projection of the magnetization on the plane: (m_1, m_2).

Bibliography

[1] T. H. R. Skyrme. Nucl. Phys., 31:56, 1962.

[2] K. Everschor-Sitte, J. Masell, R. M. Reeve, and M. Kläui. Perspective: Magnetic skyrmions—overview of recent progress in an active research field. Journal of Applied Physics, 124(24):240901, 2018.

[3] Christoph Schütte. Skyrmions and monopoles in chiral magnets and correlated heterostructures. PhD Thesis, Universitat zu Koln, 2014.

[4] Fert Albert, Nicolas Reyren, and Vincent Cros. Advances in the physics of magnetic skyrmions and perspective for technology. Unité Mixte de Physique CNRS, Thales, Univ. Paris-Sud, Université Paris-Saclay, 91767 Palaiseau, France, 06 2017.

[5] Stephen Blundell. Magnetism in condensed matter. Oxford University Press, 2001.

[6] David Bachmann. Static vortex-antivortex configurations in Dzyaloshinskii-Moriya materials. Master Thesis, 2018.

[7] Bram van Dijk. Skyrmions and the dzyaloshinskii-moriya interaction. Master Thesis, 2014.

[8] J. A. Fernandez-Roldan, A. De Riz, B. Trapp, C. Thirion M. Vazquez, J.-C. Toussaint, O. Fruchart, and D. Gusakova. Modeling magnetic-field-induced domain wall propagation in modulated-diameter cylindrical nanowires. Scientific Reports, 9:5130, 2019.

[9] Stavros Komineas, Christof Melcher, and Stephanos Venakides. Traveling domain walls in chiral ferromagnets. Nonlinearity, 32(7):2392–2412, may 2019.

[10] A. A. Belavin and A. M. Polyakov. Metastable states of 2-dimensional isotropic ferromagnets. JETP Lett., 22:245, 1975.

[11] Stavros Komineas, Christof Melcher, and Stephanos Venakides. The profile of chiral skyrmions of small radius. Nonlinearity, 33(7):3395–3408, may 2020.

[12] Stavros Komineas, Christof Melcher, and Stephanos Venakides. Chiral skyrmions of large radius. Physica D: Nonlinear Phenomena, 418:132842, 2021.

[13] D. Pinna, G. Bourianoff, and K. Everschor-Sitte. Reservoir computing with random skyrmion textures. Phys. Rev. Applied, 14:054020, Nov 2020.

[14] Xichao Zhang, Jing Xia, Motohiko Ezawa, Oleg A. Tretiakov, Hung T. Diep, Guoping Zhao, Xiaoxi Liu, and Yan Zhou. A frustrated bimeronium: Static structure and dynamics. Applied Physics Letters, 118(5):052411, 2021.